Journal of Thermal Analysis and Calorimetry (2020) 141:2429–2451
https://doi.org/10.1007/s10973-020-09412-5

Numerical study of thermo-hydraulic characteristics for forced convective flow through wavy channel at different Prandtl numbers

Sumit Kumar Mehta[1] · **Sukumar Pati**[1]

Received: 25 October 2019 / Accepted: 4 February 2020 / Published online: 21 February 2020

Abstract

The present work numerically investigates the thermo-fluidic and entropy generation characteristics for laminar forced convective flow through wavy channel at different Prandtl number (Pr). Results are presented for the following range of parameters: Reynolds number $5 \leq \mathrm{Re} \leq 200$, Prandtl number $0.72 \leq \mathrm{Pr} \leq 100$, dimensionless amplitude $0.3 \leq \alpha \leq 0.7$ and dimensionless wavelength $0.5 \leq \lambda \leq 1.5$. It is observed that with increase in Pr, the thickness of the thermal boundary layer at trough region decreases slowly for smaller Re, whereas at higher Re, the rate of decrement is higher. The average Nusselt number increases with Pr for all amplitude, wavelength and Reynolds number. The relative heat transfer enhancement compared to equivalent plane channel is presented in terms of enhancement ratio (ER), and it shows a non-monotonic variation of ER with Pr at lower Re and a monotonic one at higher Re. The combined alteration of rate of heat transfer and pressure drop as compared to plane channel is enumerated by performance factor (PF), and the variation of PF with Pr shows non-monotonic behaviour at lower Re and monotonic one at higher Re. The variation of PF shows non-monotonic variation with Re for higher Pr and for smaller wavelength, whereas it monotonically decreases for all Pr at higher wavelength. Thermal entropy generation contribution is higher over the viscous one for all the cases considered. The local thermal entropy generation distribution varies with Re, Pr and geometrical configuration of the channel. For smaller amplitude ($\alpha = 0.3$), the total entropy generation is minimum in the considered range of Re and Pr.

Keywords Wavy channel · Prandtl number · Nusselt number · Entropy generation · Bejan number

List of symbols

A	Amplitude (m)
Be	Bejan number (–)
C_p	Specific heat (J kg^{-1} K^{-1})
ER	Enhancement ratio (–)
k	Thermal conductivity (Wm^{-1} K^{-1})
L	Inlet half height (m)
N'''	Dimensionless local entropy generation (–)
N	Dimensionless total entropy generation (–)
Nu	Nusselt number (–)
$\overline{\mathrm{Nu}}$	Average Nusselt number (–)
PF	Performance factor (–)
Pr	Prandtl number (–)
Re	Reynolds number (–)
s	Wavy profile (m)
S'''	Local entropy generation rate (W K^{-1} m^3)
T	Temperature (K)
u, v	x and y-velocity component (m s^{-1})
U, V	Dimensionless x and y velocity (–)
X, Y	Dimensionless coordinate (–)

Greek symbols

α	Dimensionless amplitude (–)
ρ	Density (kg m^{-3})
μ	Dynamic viscosity (kg m^{-1} s^{-1})
θ	Dimensionless temperature (–)
Φ	Irreversibility distribution ratio (–)

Subscript

avg	Average
e	End
in	Inlet
s	Start
w	Wall

✉ Sumit Kumar Mehta
sumit090391@gmail.com

Sukumar Pati
sukumarpati@gmail.com; sukumar@mech.nits.ac.in

[1] Department of Mechanical Engineering, National Institute of Technology Silchar, Silchar 788010, India

Introduction

The continuously increasing demands of energy for different industrial applications and the higher cost of energy motivate the researchers to develop energy efficient compact thermal devices [1–6]. The losses of energy in those industrial applications are mainly due to the heat exchanging process. Accordingly, researchers have put their effort to develop compact thermal systems capable of transferring heat at a higher rate. In this context, two methods of heat transfer enhancement are commonly used for different applications: one is active method [7] and another one is passive method [8–10]. Active methods need external perturbation for the heat transfer enhancement other than the applied pumping power, and the passive methods of heat transfer enhancement include surface modification, addition of baffles [11, 12], use of obstacles in flow path, uses of twisted or helical tapes [13–15], addition of nanoparticle [16–18], porous media [19], etc. The passive heat transfer enhancement techniques are used for many heat exchanging applications, like solar water heater, nuclear reactor, and petroleum pre-heater, etc. [20–28].

Numerous works have been reported describing the effects of modification of the channel geometry to develop compact thermal devices. Rush et al. [29] experimentally investigated the heat transfer enhancement through sinusoidal passage in laminar regime and found that the local heat transfer rate enhances due to the formation of recirculation zone in the wavy part. To analyse the heat transfer mechanism in wavy channel more precisely, numerical simulations were performed by the Wang and Chen [30] for laminar regime ($100 \leq \mathrm{Re} \leq 700$) with different channel amplitudes and two different Prandtl numbers 0.72 (air) and 6.93 (water). It is found that the size of recirculation zone increases with increase in amplitude. The maxima of local Nusselt number and skin-friction coefficient exist at the peak of the wavy wall, whereas minima is located short distance downstream and upstream near to the maximum cross-sectional area. Pati et al. [31] numerically studied the thermo-hydraulic characteristics for flow through the raccoon and serpentine channels in laminar regime for Reynolds number in the range $5 \leq \mathrm{Re} \leq 100$ and $\mathrm{Pr} = 6.93$. It is found that the thermo-hydraulic performance factor is always higher for the serpentine channel in the considered range of Reynolds number and all geometrical configurations. Mehta and Pati [32] numerically investigated the effect of geometrical parameters on the thermo-hydraulic characteristics for the flow of air ($\mathrm{Pr} = 0.72$) through triangular corrugated channel. It is found that the performance factor is higher for higher amplitude ($\alpha = 0.4$) when wavelength is smaller ($\lambda = 0.5$), in the considered range of Reynolds number. For larger wavelength ($\lambda = 2$) performance factor is higher for $\alpha = 0.3$ when $\mathrm{Re} < 200$ and for $\alpha = 0.2$ when $\mathrm{Re} > 200$. Mohanraj et al. [24] reviewed different types of artificial neural networks (ANN) method to predict the heat transfer rate and friction factor for different types of heat exchanger, viz. corrugated heat exchanger, helical tubes, and straight tube with internal fins and reported that the Nusselt number for heat exchanger having corrugated channel predicted by multilayer feed forward network (MLFFN)-ANN model with 4-5-1 configuration has maximum and minimum relative difference with 10% and 0.25%, respectively; along with less than 3.36% mean relative difference. In recent times, numerous numerical and experimental investigations have been reported by various researchers on passive heat transfer techniques, which include wavy and corrugated walls, helical-twisted tapes, baffles [11–15, 30–34]. Apart from the heat transfer enhancement, the performance of the heat exchanging system should be analysed, as it is essential for the economic use of devices. In this context, Mohanraj et al. [25] experimentally studied the energy performance of heat pump with photovoltaic–thermal evaporator (PV–TE) with triangular and circular tubes configuration. They found that the triangular configuration enhances the energy performance over the circular one. The performances of a solar water heater and two-stage cascade heat pump (TSCHP) heating system have been studied numerically by Yerdesh et al. [27]. For forced convective flow through heat exchanging system with corrugated or wavy channel, pressure drop increases as compared to the plane channel. Hence, for such systems the relative enhancement of heat transfer with relative increase in pressure drop penalty as compared to the plane channel has been studied by number of researchers [31, 32].

It is important to mention here that the heat transfer for forced convective flow not only depends on the Reynolds number but also on the working fluids. Numerous works are available in the literature exploring the convective heat transfer using fluids of various kinds having different Prandtl numbers [35–42]. The common working fluids for different heat transfer processes are generally air, water, water-glycerol solutions, etc. [41]. Prandtl number for air and water is 0.72 and 6.93 [30–32], respectively, in normal atmospheric conditions, whereas for water–propylene-glycol solution Prandtl number varies from 18 to 160 [41].

The irreversibility generated during any heat exchange process is one of the parameter that decides the effectiveness of the process. The useful energy for the any heat transfer devices is destroyed by the generation of irreversibility. The useful energy for the heat exchanging system is termed as "exergy". Recently, Kumar et al. [26] and Arun et al. [28] experimentally studied the exergy analysis for the forced convective thermal system having solar air heaters using pin–fin absorber plate, and solar cabinet dryer,

respectively. According to the second law of thermodynamics, the irreversibility cannot be fully diminished, but it can be minimized [43–45]. Numerous researchers worked on to explore the entropy generation for flow through wavy channel. Akbarzadeh et al. [46] numerically studied the effect of corrugated profile on the entropy generation characteristics for laminar regime with the range of Reynolds number $400 \leq \mathrm{Re} \leq 1400$ and found that the percentage decrement in thermal entropy generation for the increase in Reynolds number from 400 to 1400 is 111%, 100%, and 116%, respectively, for sinusoidal, trapezoidal, and triangular corrugated channel. It is also found that the thermal entropy generation is dominated over the viscous contributor even at higher Reynolds number (Re = 1000). Esfahani et al. [17] numerically investigated the effect of wave number, amplitude, nano-particle volume fraction for flow through the sinusoidal wavy channel for Reynolds number in the range $300 \leq \mathrm{Re} \leq 900$ and found that the total entropy generation reduces when wave number changes from 4 to 6, and the trend is opposite when wave number changes from 6 to 8. It is also found that the thermal entropy generation decreases with increase in Reynolds number. Mehta and Pati [32] numerically found that the maxima of total entropy generation is achieved at critical Reynolds number for flow through the triangular corrugated channel for $5 \leq \mathrm{Re} \leq 500$. They reported that the critical Reynolds number decreases with an increase in wavelength and moreover for any given wavelength, there is no effect of amplitude on critical Reynolds number.

From the exhaustive literature survey as presented for forced convective flow through wavy channel, it is found that the effects of Prandtl number on the thermo-hydraulic and entropy generation performance for wavy channel have not been investigated till now. Therefore, the objective of the present work is to study the thermo-hydraulic transport characteristics along with the irreversibility analysis for the flow of different working fluids having different Prandtl numbers through the wavy channel.

Theoretical formulation

Fluid at a uniform temperature of T_{in} and uniform velocity of $\bar{u}$ enters into the channel as represented in Fig. 1. The flat part of the channel is insulated, whereas wavy wall is maintained at the constant temperature $T_{\mathrm{w}} \left(> T_{\mathrm{in}}\right)$. The equation of the wavy profile of the walls is defined as [31]:

$$s_{\mathrm{Top}}(x) = L + A \sin\left(2\pi(x - 3L)/\gamma\right) \tag{1}$$

$$s_{\mathrm{Bottom}}(x) = -L - A \sin\left(2\pi(x - 3L)/\gamma\right) \tag{2}$$

Here, L is the average half height, A is the amplitude, and γ is the wavelength of the channel.

The normalized equation of the undulated wall is given as:

$$S_{\mathrm{Top}}(X) = 1 + \alpha \sin[\pi(X - 3)/\lambda] \tag{3}$$

$$S_{\mathrm{Bottom}}(X) = -1 - \alpha \sin[\pi(X - 3)/\lambda] \tag{4}$$

Here, $S(X)$ is the normalized profile of the wavy wall, normalized as: $S(X) = s(x)/L$, $\alpha = A/L$, $\lambda = \gamma/2L$, X is dimensionless axial coordinate, normalized with L.

The flow through the wavy channel is considered to be two-dimensional, steady and incompressible [30]. Working fluid is considered as Newtonian, and for numerical analysis we consider different Prandtl numbers (=0.72, 6.93, 20, 50 and 100) [30–32, 41]. The viscous dissipation and radiation effects are neglected for the present analysis [31, 32, 46]. The temperature-independent thermo-physical properties are taken for the simulations. For the present study, the value of maximum temperature difference is less than 10 K so that we can neglect the effect of temperature on the thermo-physical properties which is in line with the previous works [30–32, 46] related to the forced convective flow through wavy channel.

The governing transport equations are presented in dimensionless form as follows [31]:*Continuity equation*:

$$\nabla \cdot \mathbf{U} = 0 \tag{5}$$

Momentum equation

$$(\mathbf{U} \cdot \nabla)\mathbf{U} = -\nabla P + (1/\mathrm{Re})\nabla^2 \mathbf{U} \tag{6}$$

Energy equation

$$\mathbf{U} \cdot \nabla\theta = \left[1/(\mathrm{Re}\ \mathrm{Pr})\right]\nabla \cdot (\nabla\theta) \tag{7}$$

where $\nabla = \left(\hat{i}\partial/\partial X + \hat{j}\partial/\partial Y\right)$ and $\mathbf{U} = \left(u\hat{i} + v\hat{j}\right)/\bar{u} = U\hat{i} + V\hat{j}$. Different normalized parameters for the above equations are: $X = x/L$, $Y = y/L$, $U = u/\bar{u}$, $V = v/\bar{u}$, $P = p/\rho\bar{u}^2$, $\theta = \left(T - T_{\mathrm{in}}\right)/\left(T_{\mathrm{w}} - T_{\mathrm{in}}\right)$,

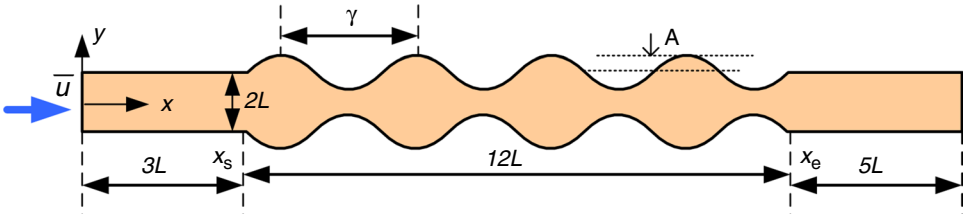

Fig. 1 Physical model and the coordinate system

where P is the normalized pressure, $\bar{u}$ is the average inlet velocity. Note that ρ, μ, k and c_p are density, dynamic viscosity, thermal conductivity and specific heat capacity of the fluid, respectively. Reynolds number and Prandtl numbers are defined as $\mathrm{Re} = (\rho \bar{u} L)/\mu$ and $\mathrm{Pr} = (\mu c_p)/k$, respectively. The imposed boundary conditions are the following:

At the inlet:

$$U = 1, \quad V = 0, \quad \theta = 0 \tag{8}$$

At the outlet:

$$\partial U/\partial X = \partial V/\partial X = \partial \theta/\partial X = 0, \tag{9}$$

At the walls:

$$U = V = 0 \tag{10a}$$

$$\theta = 1 \quad \text{for} \quad X_s \le X \le X_e \tag{10b}$$

$$\partial \theta/\partial Y = 0 \quad \text{for} \quad X < X_s \quad \text{or} \quad X > X_e \tag{10c}$$

The calculated temperature field is characterized by local Nusselt number as defined by [31]:

$$\mathrm{Nu} = -\partial \theta/\partial n \tag{11}$$

Here, n is the outward normal on the wall.

Average Nusselt number is calculated as [31]

$$\overline{\mathrm{Nu}} = \left(\int_{X=3}^{X=15} \mathrm{Nu} dS\right) \Big/ \left(\int_{X=3}^{X=15} dS\right) \tag{12}$$

Enhancement ratio (ER), pressure ratio (PR) and performance factor (PF) are calculated as [32]:

$$\mathrm{ER} = \overline{\mathrm{Nu}}_{\mathrm{wavy}} \Big/ \overline{\mathrm{Nu}}_{\mathrm{plane}} \tag{13}$$

$$\mathrm{PR} = \Delta P_{\mathrm{wavy}} \Big/ \Delta P_{\mathrm{plane}} \tag{14}$$

$$\mathrm{PF} = \mathrm{ER}/(\mathrm{PR})^{1/3} \tag{15}$$

Here ΔP is the pressure drop.

Important to mention here that flow processes through any thermal devices generate irreversibilities and accordingly to analyse the related irreversibilities associated with the heat transfer and fluid flow through the wavy channel, entropy generation analysis has been done. There are two types of irreversibilities present for the current work. First one is the thermal entropy generation caused by the local temperature gradients, and second one is the viscous or frictional entropy generation caused by the conversion of flow energy into the intermolecular energy [32, 47, 48]. The combination of local thermal equilibrium with linear transport theory, the local entropy generation for the work considered here is given by [49]:

$$S''' = \frac{k}{T_m^2}\left[\left(\frac{\partial T}{\partial x}\right)^2 + \left(\frac{\partial T}{\partial y}\right)^2\right] + \frac{\mu}{T_m}\left[2\left(\left(\frac{\partial u}{\partial x}\right)^2 + \left(\frac{\partial v}{\partial y}\right)^2\right) + \left(\frac{\partial v}{\partial x} + \frac{\partial u}{\partial y}\right)^2\right] \tag{16}$$

where T_m is the mean temperature, defined as $T_m = (T_{in} + T_w)/2$.

Here, first and second terms are called local thermal entropy generation and local viscous or frictional entropy generation, respectively. The dimensionless form of Eq. (16) can be written as:

$$N''' = \left[\left(\frac{\partial \theta}{\partial X}\right)^2 + \left(\frac{\partial \theta}{\partial Y}\right)^2\right] + \Phi\left[2\left(\left(\frac{\partial U}{\partial X}\right)^2 + \left(\frac{\partial V}{\partial Y}\right)^2\right) + \left(\frac{\partial V}{\partial X} + \frac{\partial U}{\partial Y}\right)^2\right] \tag{17}$$

Here, $\Phi = (\mu T_m/k)\left(\bar{u}/(T_w - T_{in})\right)^2$ is termed as irreversibility distribution ratio [49, 50]. When $\Phi > 1$, viscous entropy generation is dominated over the thermal entropy generation and opposite is the case for $\Phi < 1$. For the laminar flow, the value of Φ is much less than unity [51]. For the present study value of Φ is fixed and taken as 10^{-4} [51]. The dimensionless local entropy generation is normalized as $N''' = (S''')\Big/\left(k(T_w - T_{in})^2 \Big/ T_{in}^2 L^2\right)$. The volumetric total entropy generation can be calculated as [32]:

$$N_{\mathrm{Total}} = \frac{\iint_{\mathrm{Area}} N''' \Omega}{\iint_{\mathrm{Area}} d\Omega} \tag{18}$$

Here, $d\Omega$ is the elementary area of the present physical domain.

The local contribution of thermal entropy generation over the total entropy generation is defined by a term called Bejan number. Mathematically it is defined as [32, 51]:

$$\mathrm{Be} = \frac{N'''_{\mathrm{Thermal}}}{N'''_{\mathrm{Thermal}} + N'''_{\mathrm{Viscous}}} \tag{19}$$

Bejan number physically signifies the dominant contributor of entropy generation locally. If $\mathrm{Be} > 0.5$, thermal entropy generation dominates and for the case $\mathrm{Be} < 0.5$, frictional entropy generation dominates locally [32, 51].

Numerical method and model validation

Finite volume method is implemented to solve the transport equations numerically using ANSYS Fluent 14.0 [52].

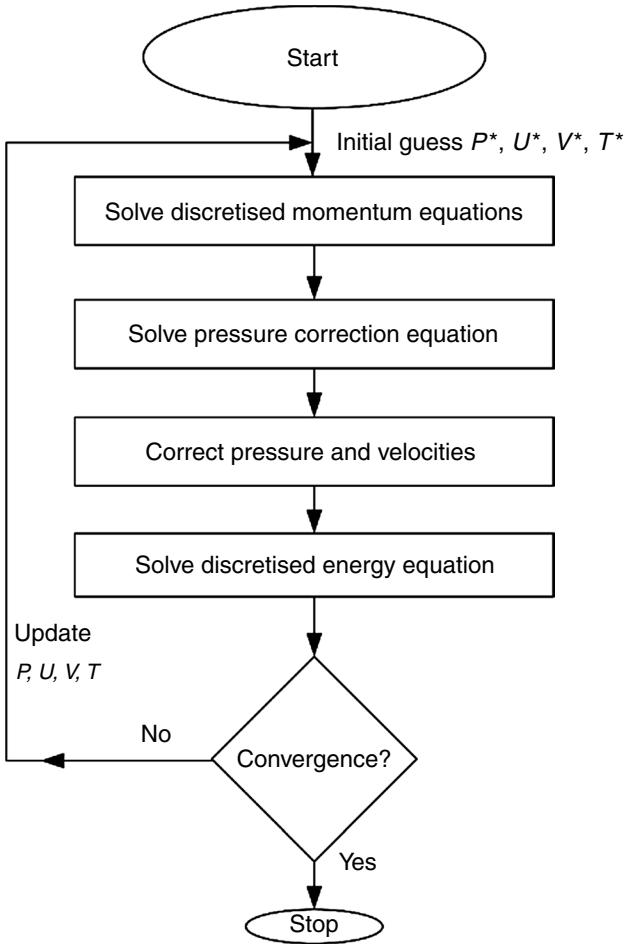

Fig. 2 Flow chart for numerical simulation

The gradients are computed by the least squares cell-based gradient evaluation method. To achieve the higher order accuracy, the momentum and energy equation are discretized by second-order upwind scheme. To take care of the pressure–velocity coupling, SIMPLE algorithm [53] is used. The flow chart for the numerical simulation procedure is presented in Fig. 2. The non-uniform mesh is considered for the numerical analysis, and mesh is dense near the wall. The relative residual criteria for convergence are taken as 10^{-6} for velocity and temperature. The grid sensitivity test has been done for all geometries to confirm that the presented results are insensitive with the grid system. The results of grid independency test for all geometries are presented in Tables 1–3 for $\lambda = 0.5,\ 1$ and 1.5, respectively, at Re = 100 and Pr = 50. It can be seen that the percentage difference in average Nusselt number is less than 0.39% compared to the very fine mesh system (M). The selected mesh systems (M) for different geometries are M3, M7, M11, M15, M19, M23, M27, M31 and M35.

Extensive validations have been done prior to conduct numerical simulations. First validation has been done to

Table 1 Grid independence test for $\lambda = 0.5$ at Re = 100 and Pr = 50

	Mesh type	No. of Elements	$\overline{Nu}$	% Difference
α=0.3	M1	73,156	13.183	3.65
	M2	103,546	12.834	0.90
	M3	213,445	12.732	0.102
	M4	356,134	12.719	–
α=0.5	M13	94,636	13.812	5.77
	M14	142,324	13.268	1.6
	M15	234,952	13.093	0.26
	M16	314,213	13.059	–
α=0.7	M25	56,156	19.118	4.81
	M26	193,282	18.331	0.5
	M27	255,496	18.266	0.14
	M28	314,197	18.24	–

Table 2 Grid independence test for $\lambda = 1$ at Re = 100 and Pr = 50

	Mesh type	No. of Elements	$\overline{Nu}$	% Difference
α=0.3	M5	71,060	12.124	7.04
	M6	113,104	11.651	2.9
	M7	200,300	11.3328	0.06
	M8	349,406	11.326	–
α=0.5	M17	77,655	13.283	8.15
	M18	126,468	12.75	3.81
	M19	223,204	12.33	0.39
	M20	306,177	12.282	–
α=0.7	M29	45,358	18.008	8.05
	M30	87,817	16.964	1.79
	M31	205,108	16.713	0.28
	M28	314,197	18.24	–

Table 3 Grid independence test for $\lambda = 1.5$ at Re = 100 and Pr = 50

	Mesh type	No. of Elements	$\overline{Nu}$	% Difference
α=0.3	M9	70,432	10.575	15.70
	M10	104,272	9.5834	4.85
	M11	199,086	9.1492	0.11
	M12	344,810	9.1391	–
α=0.5	M21	88,410	12.767	10.1
	M22	138,206	11.774	1.53
	M23	222,594	11.598	0.009
	M24	300,731	11.597	–
α=0.7	M33	41,282	16.495	6.77
	M34	84,487	15.694	1.58
	M35	202,496	15.452	0.019
	M36	339,846	15.449	–

verify the heat transfer enhancement in wavy channel. The local Nusselt number is compared with the results of Wang and Chen [30] for the sinusoidal wavy channel for Pr = 6.93, Re = 100 and $\alpha = 0.2$. Validation has also been done by comparing the results of Nusselt number for flow of water through sinusoidal channel with the experimental results of Rush et al. [29]. Both the validations have been presented in [31]. A separate validation is presented in Fig. 3a showing the variation of Nusselt number with the results of Kumar and Dhiman [54]. The result is compared for the flow of air through the backward facing step at Re = 50 and 100. The results of the present model is also compared with the experimental results of Farhanieh et al. [55] by comparing the local Nusselt number for the flow of air through the grooved channel at Re = 620 as shown in Fig. 3b. The third validation is done by comparing the local entropy generation with the results of Esfahani and Shahabi [56] for flow of higher Prandtl number fluid through the circular pipe in laminar regime. The comparison of the variation of local entropy generation at the wall of the pipe is reported in Fig. 3c for inlet velocity 0.02 m s^{-1}, dimeter of the pipe 0.025 m, length of the cylinder 1 m and Prandtl number 13,400. From the comparisons of Nusselt number and entropy generation with the reported works [29, 30, 54–56], the accuracy of the scheme used in this work is confirmed.

Results and discussions

The thermo-hydraulic and entropy generation characteristics have been studied for steady, incompressible and laminar flow of Newtonian fluid through the wavy channel by varying different parameters in the following range: Reynolds number $5 \le Re \le 200$, Prandtl number $0.72 \le Pr \le 100$, dimensionless amplitude $0.3 \le \alpha \le 0.7$ and dimensionless wavelength $0.5 \le \lambda \le 1.5$) [30–32, 46, 57–59].

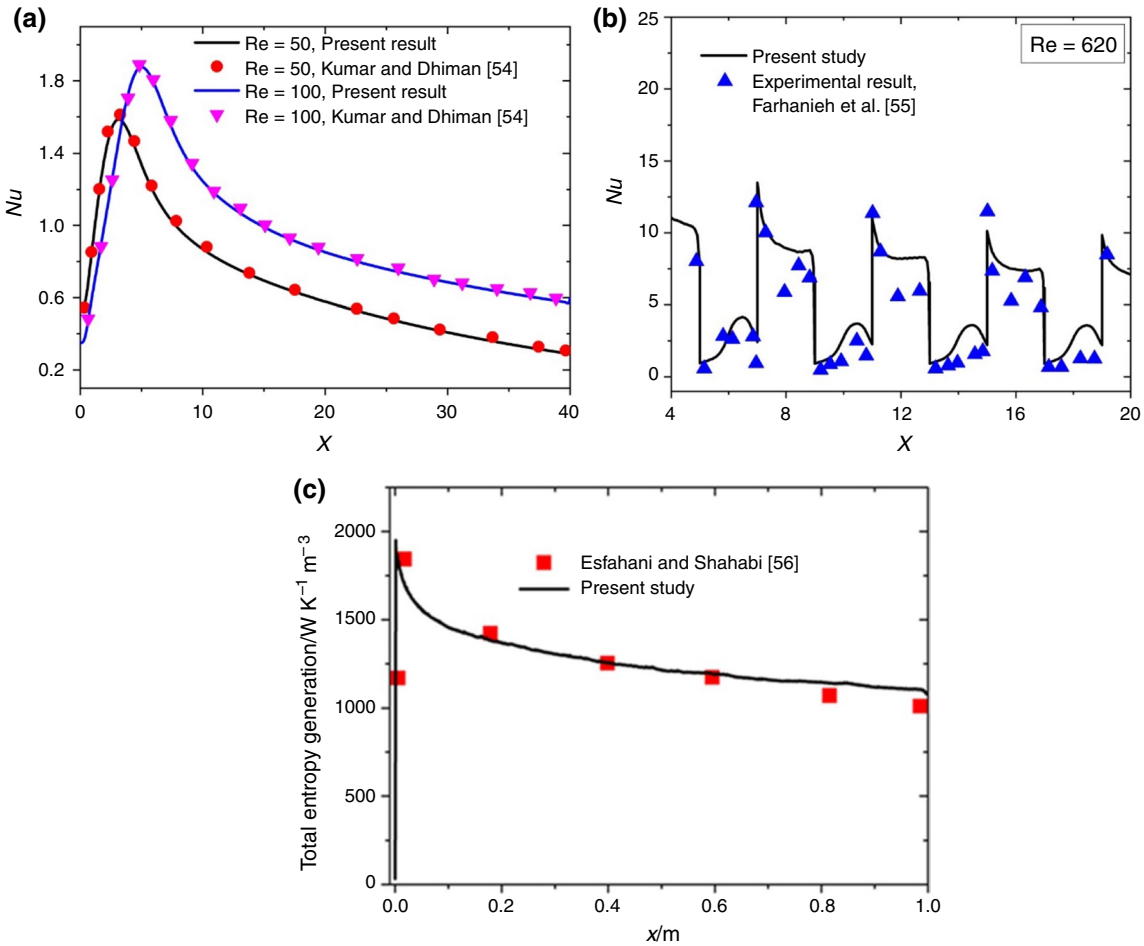

Fig. 3 **a** Comparison of local Nusselt number for the present case with the numerical results of Kumar and Dhiman [54] for the forced convective flow through the backward facing step at Pr = 0.71 and, Re = 50 and 100, **b** Comparison of local Nusselt number with the experimental results of Farhanieh et al. [55] for the forced convective flow of air through the grooved duct at Re = 620. **c** Comparison of local entropy generation at the wall of circular pipe with the results of Esfahani and Shahabi [56] for inlet velocity of 0.02 m s^{-1} and diameter of 0.025 m

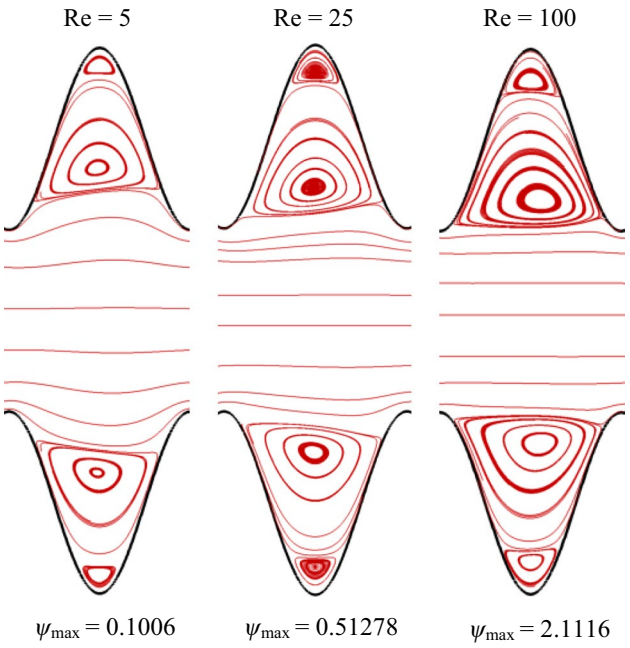

Fig. 4 Contours of streamlines for Re = 5, 25 and 100 (left to right) at $\alpha = 0.5$, $\lambda = 0.5$

To understand the flow physics for flow through the wavy channel, contours of streamlines are presented in Fig. 4 for Re = 5, 25 and 100. The wavy diverging section allows flow in the direction of adverse pressure gradient, and there is a flow reversal when the momentum loss is higher, thereby forming recirculation zone [57–60]. When the amplitude of the wavy wall is larger and wavelength is smaller (e.g., $\alpha = 0.5$ and $\lambda = 0.5$), a tertiary flow zone is also formed at the tip part of the trough as can be seen from Fig. 4 because of the excessive momentum loss. With the increase in Re, the size of the recirculation zone and strength of the vortices formed increase as the advection strength increases. The recirculation zone enhances the fluid mixing [32, 54, 55], and hence there is an increase in heat transfer rate.

To understand the variation of temperature field in the wavy channel for different Prandtl number and Reynolds number, isotherms contours are presented for Pr = 6.93 and 100 for Re = 5, 25 and 100 in Fig. 5. For any given Prandtl number, the increase in Reynolds number results in the gravitation of smaller values of isotherms towards the hot wall. This is because of the fact that as increase in the advection strength allows more cold fluid in the core region. On the other hand, at higher Reynolds number, the higher strength of the recirculation zone allows more cold fluid to flow in

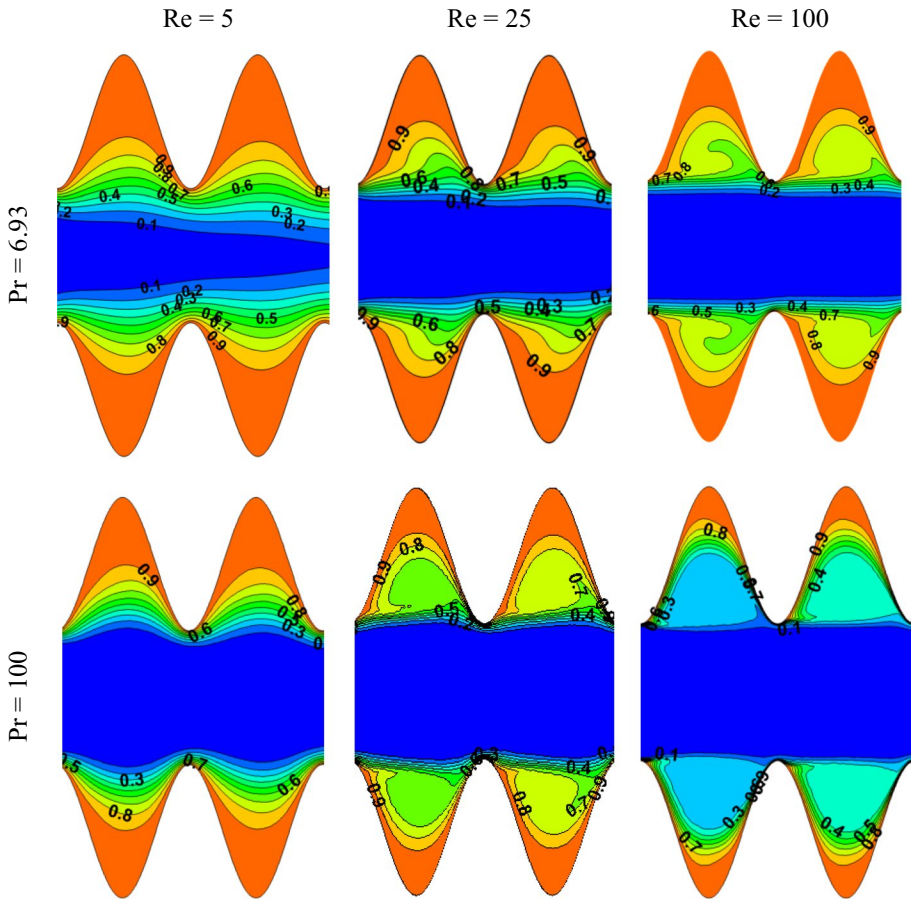

Fig. 5 Isotherms contours for Pr = 6.93 (top) and 100 (bottom) for Re = 5, 25 and 100 (left to right) at $\alpha = 0.5$, $\lambda = 0.5$

the trough region. At the tip region, intensity of isotherms is very high due to the presence of tertiary flow region. The increase in Prandtl number allows easier transport of heat for a given convection strength as thermal Peclet number (Pe_T) increases. In other words, the increase in Prandtl number allows to decrease the thermal boundary layer thickness (TBL) as for flat surface $(TBL/L) \sim \left(1/Pe_T\right)^{0.5}$ or $(TBL/L) \sim (1/(Re\ Pr))^{0.5}$ [61]. Therefore, the attraction of smaller values of isotherms towards the hot wall is higher at higher Re and Pr.

The local heat transfer enhancement can be represented by local Nusselt number, and the corresponding variation at top wall of the channel is presented in Fig. 6 at two different Reynolds numbers (Re = 5 and 100) for different values of Prandtl numbers.

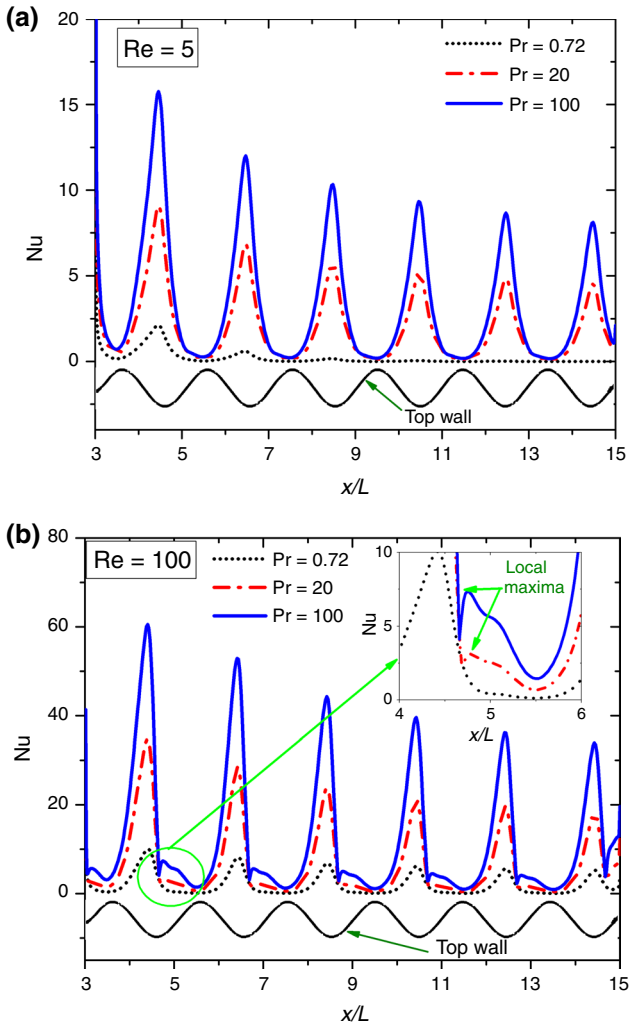

Fig. 6 Variation of local Nusselt number along the top wavy wall for different values Prandtl number at **a** Re = 5 and **b** Re = 100. The additional local maxima of local Nusselt number at higher Pr (= 20 and 100) and Re = 100 can be seen in zoomed view in the inset

Two Reynolds numbers are so chosen such that at lower Reynolds number (Re = 5) no recirculation zone is formed and at higher Reynolds number (Re = 100) recirculation zones are formed on the wavy part of the channel. Figure 6a depicts the local Nusselt number variation at top wall for different Pr (= 0.72, 20 and 100) at $\alpha = 0.5$ and $\lambda = 1$. At Pr = 0.72, high value of Nusselt number is found near the inlet side throat region and beyond the first two wavelength of upstream side, local Nusselt number approaches the zero. This is happened because the hot fluid is present near the hot wall for the combination of smaller Reynolds number and Prandtl number as discussed (see Fig. 5), whereas a high value of Nusselt number is obtained near the inlet side because of the effect of cold fluid and higher velocity gradient at throat. For Pr = 20 and 100, the frequency of the local minima and maxima of local Nusselt number is same as the wavy wall profile. The local minima of Nusselt number exists at the trough section, whereas maxima exists at the throat. It can be explained from the fact that the flow retardation takes place at trough, while at throat the flow is accelerated because of the change in the flow path area. It can be noted that the local maxima of local Nusselt number decreases in downstream direction, whereas minima of local Nusselt number is almost invariant. It is because of the enhancement in mean temperature of fluid increases the thermal boundary layer thickness in equivalent wavy cross section for upstream wavelengths at the throat where flow is accelerated. Hence, the maxima of local Nusselt number at throat decreases in downstream direction, whereas at trough fluid deceleration and higher temperature intensity approaches zero heat transfer rate. The increase in Prandtl number increases the maxima of local Nusselt number and no such effect of Prandtl number is found for local minima. It is because the increase in Prandtl number decreases the thermal boundary layer thickness at throat, and the thermal boundary layer thickness becomes almost invariant at trough. Figure 6b depicts the variation of local Nusselt number at Re = 100 at top wall for Pr = 0.72, 20 and 100 with $\alpha = 0.5$ and $\lambda = 1$. For this case, the attachment and detachment of the primary flow with hot wall play an important role for the local variation of Nusselt number. Before the throat, local Nusselt number starts increasing in downstream direction up to the primary flow attachment point just before the throat and attains maxima as the attachment of primary cold flow enhances the heat transfer rate. Beyond this point, local Nusselt number decreases up to the primary flow detachment point. Before primary flow detachment point, local Nusselt number variation is same for all Prandtl number. Before primary flow detachment point, local Nusselt number is invariant in downstream direction up to the next primary flow reattachment point for Pr = 0.72, whereas for Pr = 20 and 100, local Nusselt number increases due to the flow of reversed cold secondary flow attachment along

the hot wall and attains local maxima (see inset of Fig. 6b). For Pr = 0.72, the reversed secondary flow is not so cold due to the poor capacity of heat transfer as thermal Peclet number is small. Beyond the new local maxima, local Nusselt number decreases up to the trough. Hence, for higher values of Reynolds number and Prandtl number additional local maxima and minima are induced. For Re = 100, the increase in Prandtl number increases the minima of local Nusselt number due to the presence of recirculation zone and moreover the temperature intensity depends on the Prandtl number. Hence, the corresponding change in thermal boundary layer at trough enhances the local Nusselt number with Prandtl number.

The effect of Prandtl number on average Nusselt number for different Reynolds numbers is presented in Fig. 7 for $\alpha = 0.3$ and $\lambda = 1$. Increase in Reynolds number enhances the advection strength, and increase in Prandtl number allows easier heat transfer for a given advection strength; therefore, average Nusselt number increases with the increase in Reynolds number and Prandtl number for a given geometrical parameter.

The relative enhancement of heat transfer rate as compared to the plane channel is expressed in terms of enhancement ration (ER), and corresponding variation of ER with Prandtl number at different wavelengths is presented in Fig. 8 for two different Reynolds numbers (Re = 25, left side) and (Re = 100, right side) with different amplitudes ($\alpha = 0.3$ to 0.7, top to bottom). For all cases, the value of ER is greater than unity signifying that an enhancement of overall heat transfer rate is obtained in wavy channel over the plane channel because of better fluid mixing. For lower Reynolds number (= 25), ER initially increases with Prandtl number and attains a maxima at critical Prandtl number (Pr_c)

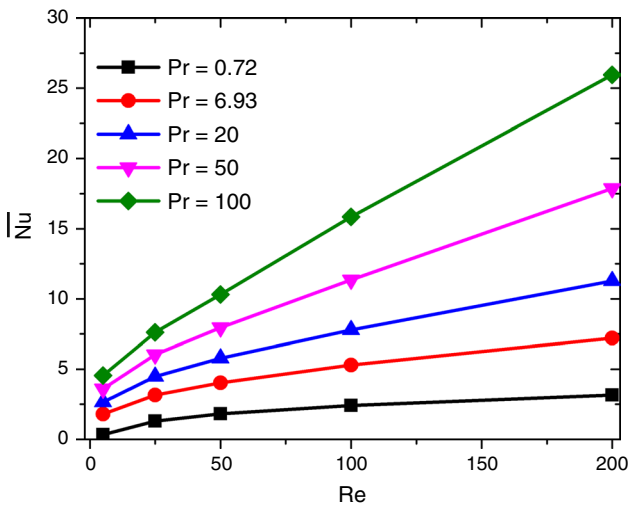

Fig. 7 Average Nusselt number versus Re at different Pr numbers with $\alpha = 0.3$ and $\lambda = 1.0$

and then decreases with increase in Pr. The slope of decrement of ER with Prandtl number increases with α or λ. This variation of ER with Prandtl number can be explained from the following parameters: strength of recirculation zone, increase in size of recirculation zone with α, increase in the number of recirculation zone with decrease in λ and the corresponding change in thermal boundary layer thickness (TBL) for the plane and wavy channel. The smaller strength of recirculation zone at lower Reynolds number causes trapping of larger quantity of hot fluid in the trough region which causes resistance in heat transfer. The increase in Prandtl number causes only minor decrement of hot fluid trapping region area (see Fig. 5 at Re = 5). For the throat region, the decrement of TBL thickness is higher and heat transfer rate enhances in this region with a larger rate with increase in Prandtl number, whereas for plane channel, the absence of recirculation zone causes uniform decrement of TBL thickness with Prandtl number. Hence, for lower Prandtl number, ER shows an increasing trend as the thicker TBL in the plane channel is the main cause of the increase in ER, whereas at higher Prandtl number, the thickness of TBL for the plane channel is narrower and for wavy channel narrowness increases significantly only at throat for lower Reynolds number. Hence, ER decreases at higher Pr. The increase in amplitude increases the size of the recirculation zone and hence increases the fluid mixing and the decrement slope of ER decreases with increase in α, whereas the decrement of wavelength increases the undulation, thereby decreasing the size of the recirculation zone and also increases the number of hot fluid trapping zone. Hence, the resistance to heat transfer rate increases and it leads to increase the slope of decrement of ER curve with decrease in λ. The value of Pr_c is constant for all wavelength for a given α and increases with α. For example, at $\alpha = 0.3$ and 0.7, the values of Pr_c are 6.93 and 20, respectively, for Re = 25. It can be explained by the fact that the higher mixing at higher amplitude results in increase of ER up to higher value of Pr. At higher Re (= 100), the extent of increasing ER takes place for all values of Prandtl number because of the fact that the strength of recirculation zone is very high at higher Reynolds number,. For example, at $\alpha = 0.5$ and $\lambda = 0.5$, the recirculation zone strength increases 4.11 times when Reynolds number changes from 25 to 100 (see the value of ψ_{max} in Fig. 4). Hence, ER monotonically increases with Prandtl number at Re = 100 for all geometrical configuration. It is important to mention that the difference in ER at different λ increases for given α and with increase in α, the rate of increment amplifies to a large extent.

To analyse the percentage enhancement in heat transfer rate in wavy channel compared to the plane channel, the percentage difference in average Nusselt number $\left(\Delta\overline{\mathrm{Nu}}\%\right)$ is presented in Table 4 for different Reynolds numbers,

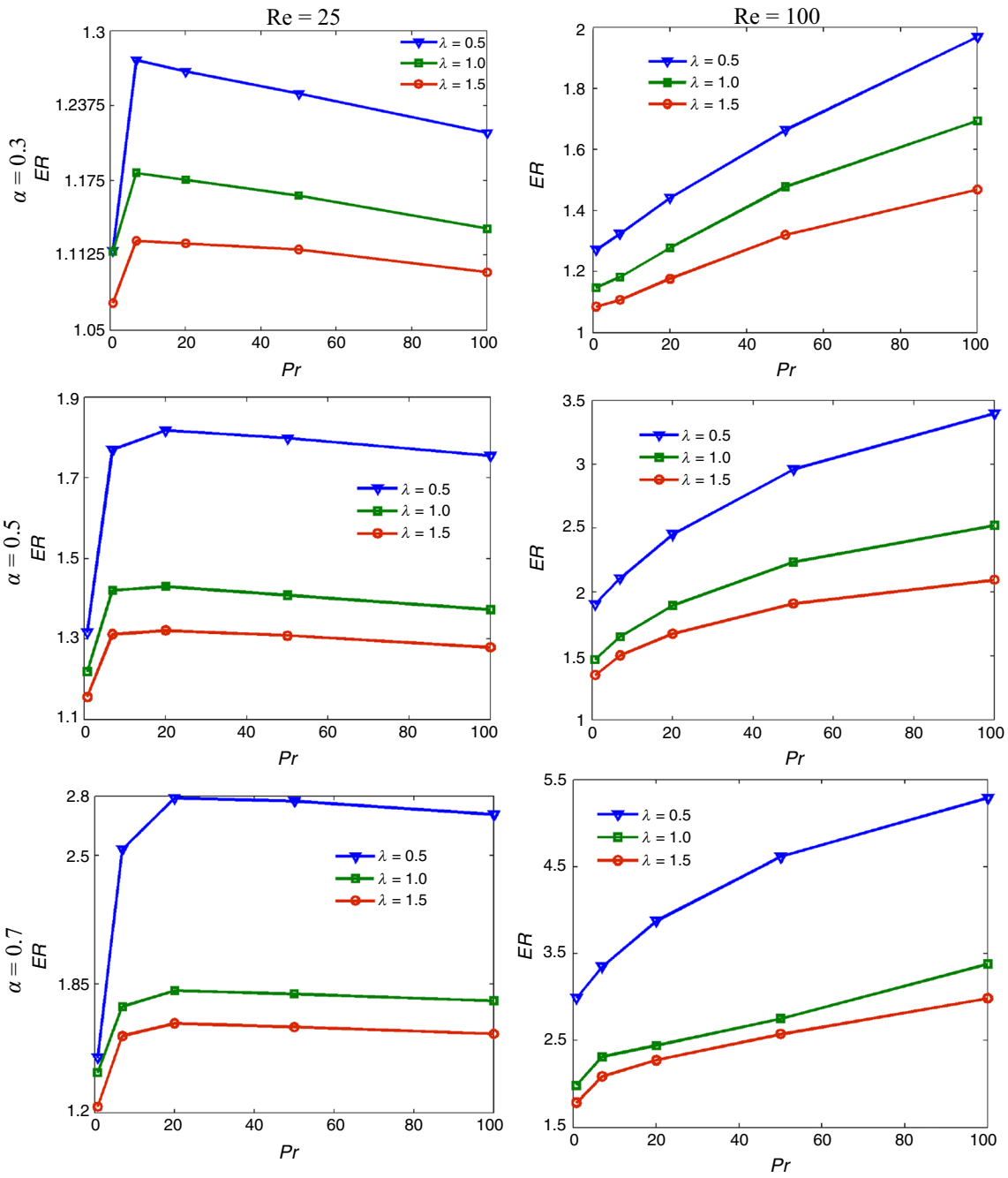

Fig. 8 Enhancement ratio versus Prandtl number for different values of wavelength for Re = 25 (left) and 100 (right) for $\alpha = 0.3$, 0.5 and 0.7 (top to bottom)

Prandtl numbers, normalized amplitude and wavelength. The mathematical representation of $\Delta\overline{\mathrm{Nu}}\%$ is defined as $\Delta\overline{\mathrm{Nu}}\% = 100\left(\overline{\mathrm{Nu}}_{\mathrm{wavy}} - \overline{\mathrm{Nu}}_{\mathrm{plane}}\right)\Big/\overline{\mathrm{Nu}}_{\mathrm{plane}}$. It can be seen from the table that the variation of $\Delta\overline{\mathrm{Nu}}\%$ is non-monotonic with Re for lower amplitude ($\alpha = 0.3$) and monotonic for higher amplitude ($\alpha = 0.5$ and 0.7). For $\alpha = 0.3$, at lower value of Prandtl number (Pr = 0.72), $\Delta\overline{\mathrm{Nu}}\%$ increases with Re monotonically at the lower wavelength ($\lambda = 0.5$), whereas for the higher values of wavelength ($\lambda = 1$ and 1.5), it increases up to Re = 50 and small reduction is observed beyond this limit. This observation can be explained as follows. The smaller wavelength allows higher undulation, and it causes higher rate of enhancement of $\overline{\mathrm{Nu}}$ for wavy channel compared to the plane channel for all Re, whereas for the higher wavelength, the smaller undulation allows higher rate of enhancement in $\overline{\mathrm{Nu}}$ for wavy channel up to Re = 50, and

Table 4 Percentage difference in average Nusselt number for wavy channel compared to the equivalent plane channel $\left(\Delta\overline{\mathrm{Nu}}\%\right)$ for different Prandtl numbers, Reynolds numbers, amplitude and wavelength

$$\Delta\overline{\mathrm{Nu}}\% = 100\left(\overline{\mathrm{Nu}}_{\mathrm{wavy}} - \overline{\mathrm{Nu}}_{\mathrm{plane}}\right)\Big/\overline{\mathrm{Nu}}_{\mathrm{plane}}$$

	Re	$\alpha=0.3$			$\alpha=0.5$			$\alpha=0.7$		
		$\lambda=0.5$	$\lambda=1$	$\lambda=1.5$	$\lambda=0.5$	$\lambda=1$	$\lambda=1.5$	$\lambda=0.5$	$\lambda=1$	$\lambda=1.5$
Pr = 0.72	5	11.60	11.56	7.25	31.60	21.88	15.63	47.89	40.23	23.09
	25	22.88	15.74	10.22	62.96	34.66	25.41	116.64	57.89	45.34
	50	26.65	16.93	10.93	79.32	42.33	31.11	164.78	80.76	64.62
	100	27.47	16.18	10.09	87.93	46.21	34.09	198.94	98.25	78.34
Pr = 20	5	26.60	17.56	12.23	81.77	43.05	32.11	179.07	81.79	65.20
	25	24.48	12.97	8.12	85.48	46.98	32.94	203.09	108.76	87.03
	50	26.18	13.63	7.27	93.78	55.91	39.84	235.76	127.50	105.43
	100	31.33	17.35	9.50	111.52	68.27	49.28	287.70	144.04	127.16
Pr = 100	5	21.46	13.45	9.82	75.44	37.28	27.93	170.77	76.59	59.91
	25	23.81	10.51	5.81	92.96	56.51	37.43	255.80	144.21	114.66
	50	32.07	16.34	7.50	127.97	84.58	59.16	353.19	194.28	157.19
	100	56.60	37.07	21.63	181.00	117.87	84.12	428.93	237.90	198.60

beyond that the rate of increase in $\overline{\mathrm{Nu}}$ for wavy channel reduces as the higher strength of recirculation zone with smaller Pr creates higher intensity of hot spot (see Fig. 5) and resists the heat transfer enhancement. For $\alpha = 0.3$, at Pr = 20, the value of $\Delta\overline{\mathrm{Nu}}\%$ decreases with Re up to some critical value and again increases for all wavelength. It can be explained as follows. The absence of recirculation zone along with the easier heat transfer rate due to the higher Pr (= 20) and fluid acceleration at throat at lower Re allows higher heat transfer rate in wavy channel, whereas with increase in Re, the deceleration and formation of smaller strength of recirculation zone up to that critical Re resist the rate of increase in $\overline{\mathrm{Nu}}$ for wavy channel compared to the plane channel. Hence, decrement in $\Delta\overline{\mathrm{Nu}}\%$ is found up to that critical Re, whereas at higher Re, the higher strength of recirculation zone enhances the fluid mixing and enhances the rate of increment in $\overline{\mathrm{Nu}}$ for wavy channel. Therefore, $\Delta\overline{\mathrm{Nu}}\%$ increases at higher Re for $\alpha = 0.3$ and Pr = 20. For the case of $\alpha = 0.3$ and Pr = 100, the variation of $\Delta\overline{\mathrm{Nu}}\%$ with Re is same as the above discussed case for higher wavelength ($\lambda = 1$ and 1.5), whereas for smaller wavelength ($\lambda = 0.5$), $\Delta\overline{\mathrm{Nu}}\%$ increases monotonically with Re as the rate of reduction in $\overline{\mathrm{Nu}}$ due to the deceleration of fluid at trough is compensated with the enhancement due to the fluid acceleration at the throat by higher undulation. It can be noted that at smaller Re (=5) the value of $\Delta\overline{\mathrm{Nu}}\%$ increases with Pr when it changes from 0.72 to 20, whereas decrement is found when Pr changes from 20 to 100 for all amplitude and wavelength. This can be explained by the fact that the thin thermal boundary layer at higher Pr for the plane channel has triggered the corresponding heat transfer rate, whereas the absence of recirculation zone at lower Re (=5) enhances the rate of heat transfer at throat due to the fluid acceleration; however, the stagnant hot spot (with change in Pr) at lower Re (see Fig. 5) reduces the rate of increase in heat transfer rate for wavy channel. Hence, $\Delta\overline{\mathrm{Nu}}\%$ reduces for Re = 5 when Pr changes from 20 to 100. For the higher amplitude ($\alpha = 0.5$ and 0.7) the value of $\Delta\overline{\mathrm{Nu}}\%$ increases with Re monotonically for all wavelength as the higher amplitude enhances the rate of increment of $\overline{\mathrm{Nu}}$ for wavy channel. It can be also noted that the value of $\Delta\overline{\mathrm{Nu}}\%$ increases with α and decreases with λ. The maximum value of $\Delta\overline{\mathrm{Nu}}\%$ is found for $\alpha = 0.7$ at Pr = 100. For higher amplitude, the value of $\Delta\overline{\mathrm{Nu}}\%$ is more than 100% for some cases (smaller wavelength and higher Re).

The effect of pressure drop penalty in wavy channel is presented in terms of pressure ratio (PR). It is the ratio of pressure drop at outlet in wavy channel to the corresponding pressure drop in plane channel. The variation of PR with Re is presented in Table 5 for different wavelengths and $\alpha = 0.3,\ 0.5$ and 0.7. It can be seen that the increase in amplitude or decrease in wavelength increases the value of PR for all Re. It is because the increase in amplitude or decrease in wavelength increases the flow resistance and increases the need of pumping power to maintain the given advection strength (i.e., given Re). The value of PR is always more than unity indicating that the pumping power requirement for wavy channel is always more than that for the equivalent plane channel. It can be noted that PR increases with Re for lower value of Re up to the critical limit and beyond this limit PR decreases with Re. It can be explained that for the lower value of Re, the rate of increment of pressure drop in wavy channel is higher as compared to plane channel and hence the increasing trend of PR is found at lower Re, whereas at the higher value of Re the rate of increment of pressure drop in wavy channel is nearly similar to the rate of increment in pressure drop for

Table 5 Variation of Pressure ratio (PR) at different amplitudes (α) and wavelength (λ)

Re	PR = $\Delta P_{wavy} / \Delta P_{plane}$								
	$\alpha = 0.3$			$\alpha = 0.5$			$\alpha = 0.7$		
	$\lambda = 0.5$	$\lambda = 1$	$\lambda = 1.5$	$\lambda = 0.5$	$\lambda = 1$	$\lambda = 1.5$	$\lambda = 0.5$	$\lambda = 1$	$\lambda = 1.5$
5	2.27	1.84	1.62	5.42	3.97	3.28	18.78	12.36	9.88
25	2.61	2.22	1.99	6.66	5.39	4.60	25.07	18.92	15.58
50	3.43	3.00	2.71	8.99	7.63	6.69	33.97	27.35	23.25
100	3.31	2.99	2.74	8.80	7.81	7.05	32.66	27.80	24.50
200	1.84	1.71	1.59	4.98	4.58	4.22	18.09	16.17	14.64

the plane channel (even the pressure drop in wavy channel is much higher in the plane channel). Hence, the overall effect decreases the value of PR at higher Re.

The wavy channel gives higher heat transfer rate at the cost of increase in pressure drop due to the flow retardation at trough as well as by flow reversal in the diverging part of the channel. Hence, the combined effect of relative

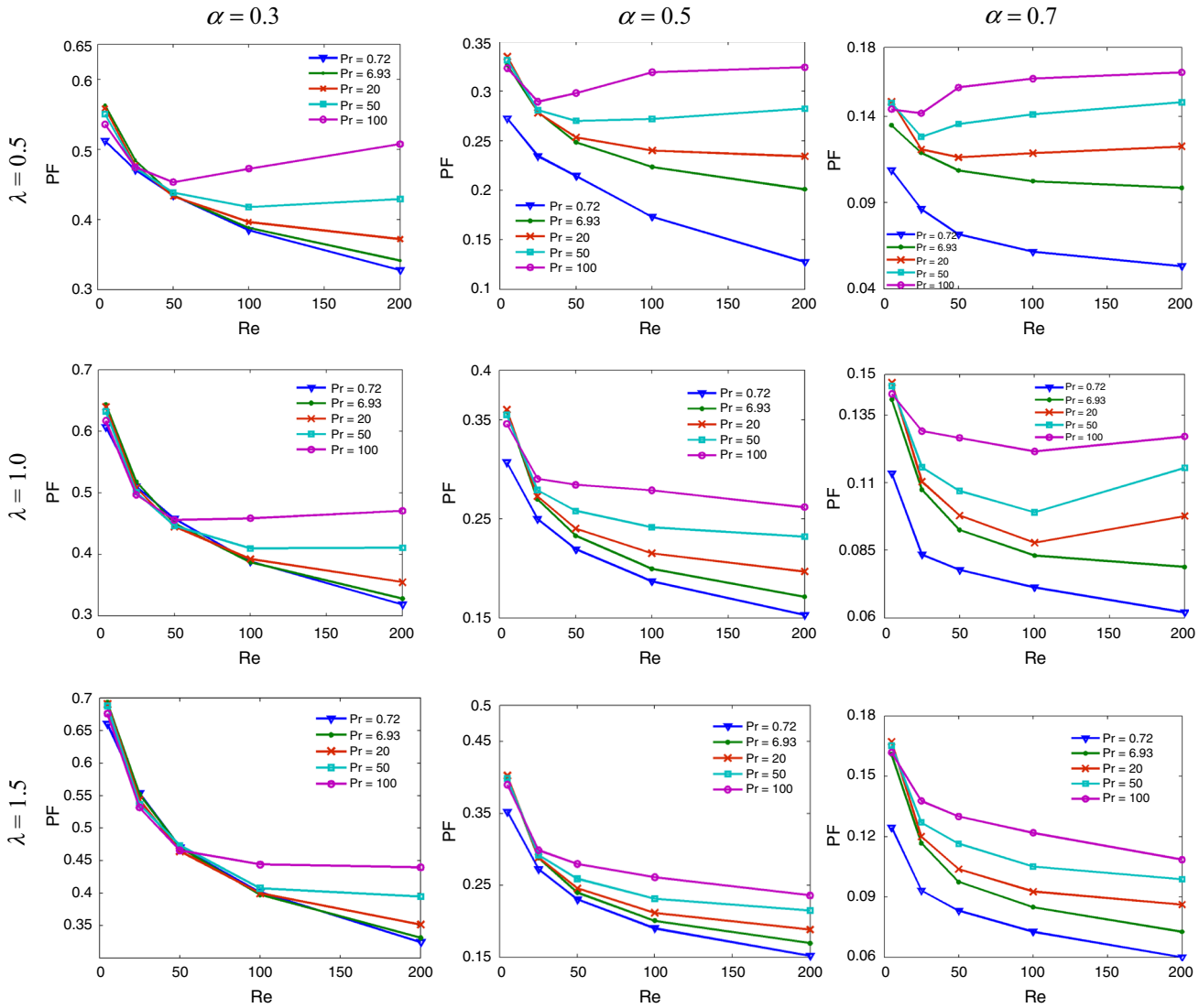

Fig. 9 Performance factor versus Re for different values of Pr for $\alpha = 0.3$ to 0.7 (left to right) and $\lambda = 0.5$ to 1.5 (top to bottom)

enhancement in heat transfer rate with an increase in relative pressure drop as compared to equivalent plane channel is analysed in terms of performance factor (PF). The variation of PF with Reynolds number at different Prandtl numbers is presented in Fig. 9 for different geometrical configurations. For a given Prandtl number, the increase in α or the decrease in λ decreases the PF as pressure drop penalty is significant over the enhancement in heat transfer rate due to the flow reversal. It is interesting to see that at lower Reynolds number, PF shows non-monotonic trend with change in Prandtl number, whereas at higher Reynolds number, the variation is monotonic and it increases with Prandtl number for a given configuration of the geometry. It is because of the non-monotonic variation of ER with Prandtl number at lower Reynolds number and monotonic variation at higher Reynolds number and the relative pressure drop monotonically increases with Reynolds number. It is important to mention that for a given α, the decrease in λ causes non-monotonic behaviour of PF variation with Reynolds number at higher values Prandtl number and PF decreases up to critical Reynolds number (Re_c) and increases again. This increment is due to the higher values of ER at higher Prandtl number compared to relative pressure drop. The value of Re_c shows a decreasing trend with increase in α. It is because the increase in amplitude allows stronger recirculation zone at smaller Reynolds number, thereby increasing the heat transfer. It is important to mention that the use of water-glycerol solutions with higher Prandtl number (Pe = 100) allows higher performance factor with higher heat transfer enhancement rate at the higher value of Reynolds number compared to the use of pure water. It can be noted that Pati et al. [31] concluded that for water (Pr = 6.93) as a working fluid, the value of performance factor decreases with Reynolds number, whereas present study predicts the increasing trend of performance factor at higher value of Reynolds number for the higher value of Prandtl number. Similarly, Mehta and Pati [32] concluded that flow of air (Pr = 0.72) through the triangular corrugated channel decreases the performance factor for higher Reynolds number. Therefore, present result suggests that the use of fluid having higher Prandtl number is better even for higher Reynolds number for forced convective flow through wavy channel.

Figure 10 depicts the distribution of dimensionless local thermal entropy generation ($N'''_{Thermal}$) for different Prandtl number at two Reynolds number (Re = 25 and 100) with fix geometrical parameter $\alpha = 0.5$ and $\lambda = 1$. For all cases, $N'''_{Thermal}$ is higher near the throat section, as higher fluid

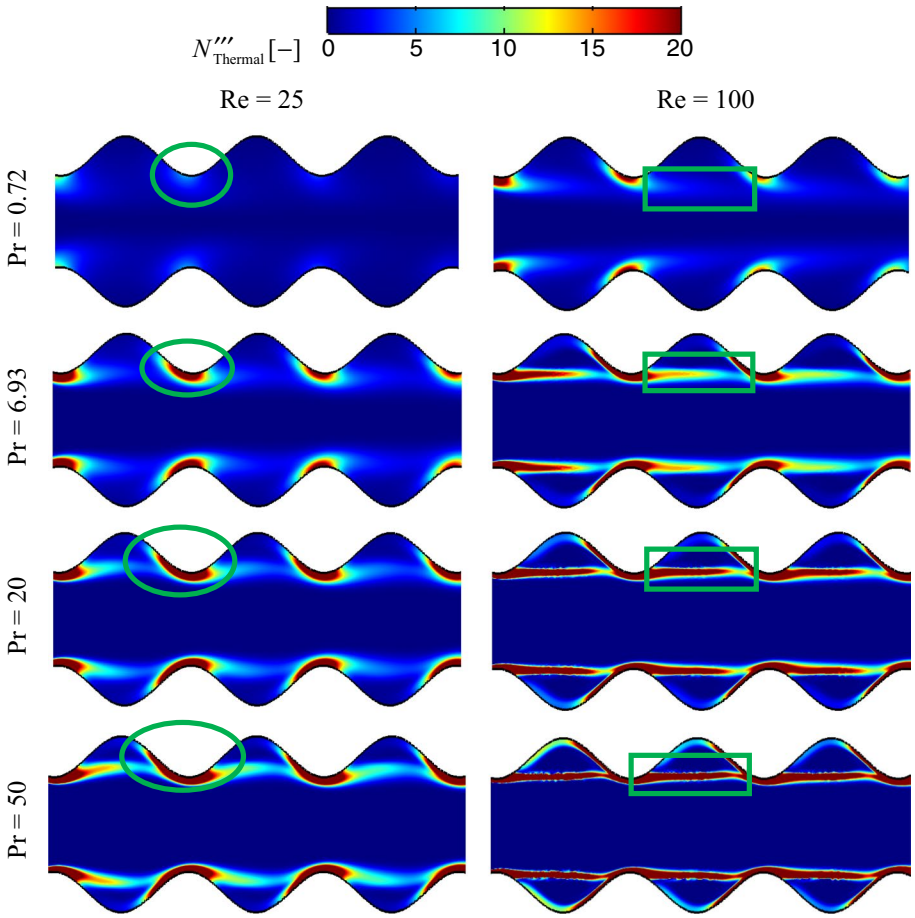

Fig. 10 Dimensionless thermal entropy generation contour for different Prandtl numbers (Pr = 0.72, 6.93, 20 and 50) at $\alpha = 0.5$ and $\lambda = 1$ for two values of Reynolds number: smaller Reynolds number (Re = 25, left side) and higher Reynolds number (Re = 100, right side)

acceleration at this region enhances the temperature gradient, whereas with increase in Prandtl number, the region of this maxima intensity develops along the wavy wall towards the upstream converging section. It is shown by the green ellipse for the case of Re = 25. This is because of the effect of primary cold flow attachment and flow acceleration by converging cross section, along with the easiness in heat transfer by increase in thermal Peclet number. For Re = 100, relative large value of N'''_{Thermal} exists at diverging section for Pr = 20 and 50. Again, this intensity increases, when Prandtl number increases from 20 to 50. The existence of large value of N'''_{Thermal} in diverging section is due to the decrease in temperature of recirculation zone at higher values of Prandtl number (see Fig. 5). Hence, the diverging section also has significant temperature gradient due to the hot wall and relatively cold recirculation zone at higher values of Prandtl number. The core region of the channel has zero intensity of N'''_{Thermal} because the inlet cold fluid gives rise to zero temperature gradient. This zero thermal entropy generation zone increases with increase in Reynolds number or Prandtl number. For a given Prandtl number, the increase in advection strength with Reynolds number allows more cold fluid to flow in the core region, whereas for a given Reynolds number, increase in Prandtl number allows easier advective transport of thermal energy and less heat accumulation in the domain. Therefore, penetration of temperature gradient towards the core decreases at higher Prandtl number. Hence, the increase in Prandtl number or Reynolds number allows to increase the core zero thermal entropy region. The effect of interaction between primary and secondary flow on N'''_{Thermal} distribution is summarized below. The secondary flow exists near the hot wall. Therefore, its temperature is relatively higher compared to the primary flow. Hence, the interaction between these two flows allows to increase the temperature gradient. This is shown by green rectangular box for the case of Re = 100. Whether, this temperature gradient is significant or not, it depends on both Reynolds number and Prandtl number. For smaller Reynolds number the smaller secondary flow strength increases the uniformity of temperature between two flows and for smaller Prandtl number, the poor heat transfer allows more heat accumulation in the domain and hence increases the uniformity of temperature between two flows. Both cases allow smaller intensity of N'''_{Thermal} at interface region. For example, no interfacial intensity of N'''_{Thermal} is found for Re = 25 and Pr = 0.72, even though the presence of recirculation zone. It is also noted that, for other cases (except Pr = 0.72 and Re = 25), the increase in Reynolds number and Prandtl number decreases the thickness of interfacial N'''_{Thermal} region. It can be explained by the fact that there is an increase in temperature uniformity in recirculation zone with increase in Reynolds number or Prandtl number (see Fig. 5). Hence, the jump of temperature difference from secondary to primary flow zone is abrupt for higher Reynolds number and Prandtl number allows narrow and higher magnitude of interfacial value of N'''_{Thermal}. The existence of temperature uniformity in the secondary flow zone allows nearly zero N'''_{Thermal}.

The effect of amplitude and wavelength on N'''_{Thermal} distribution is presented in Fig. 11 for Pr = 100 and = 6.93 with Re = 100. The effect of amplitude on N'''_{Thermal} is presented in Fig. 11a. For Pr = 6.93, the increase in amplitude allows higher intensity of interfacial value (for primary and secondary flow) of N'''_{Thermal} and the thickness of interfacial (for primary and secondary flow) N'''_{Thermal} region decreases, whereas for Pr = 100, the intensity of interfacial (for primary and secondary flow) N'''_{Thermal} is same and thickness of the region decreases with increase in amplitude. It can be noted that the existence of tertiary flow zone for $\alpha = 0.7$ allows another interfacial N'''_{Thermal} region for Pr = 100, as shown by green ellipse. At Pr = 6.93, additional interfacial region of N'''_{Thermal} is not formed even for the same amplitude due to the smaller gradient of temperature. For Pr = 100 and $\alpha = 0.3$, converging and diverging sides of wavy wall have significant value of N'''_{Thermal} continuously along the wavy surface, whereas for Pr = 100 and $\alpha = 0.7$, there is a break up of significant N'''_{Thermal} region at wavy wall for trough region (shown in green rectangle). It is because of the existence of tertiary flow zone. As the tertiary flow zone is close to the wall, the temperature of this zone is very high and uniform. Therefore, zero temperature gradient allows to generate zero thermal entropy region. The effect of wavelength on N'''_{Thermal} distribution is presented in Fig. 11b. For Pr = 6.93, the distribution of N'''_{Thermal} is same for both $\lambda = 0.5$ and 1.5; only the frequency of similar pattern of N'''_{Thermal} is higher for $\lambda = 0.5$ in given length of the channel. For Pr = 100, the distribution of N'''_{Thermal} is different for $\lambda = 0.5$ and 1.5. For this case, at $\lambda = 0.5$, the existence of tertiary flow zone breaks the N'''_{Thermal} distribution near the wall (shown in green rectangle) and continuous for $\lambda = 1.5$, due to the absence of tertiary flow zone.

The distribution of dimensionless viscous entropy generation $\left(N'''_{\text{Viscous}}\right)$ at different amplitude is presented in Fig. 12 for $\lambda = 0.5$ and Re = 100. It can be noted that for present study we fix the value of irreversibility distribution ratio (Φ). Therefore, N'''_{Viscous} is invariant with change in Prandtl number. The intensity of N'''_{Viscous} is higher only at throat for $\alpha = 0.3$, whereas for higher amplitude ($\alpha = 0.5$ and 0.7), the higher intensity of N'''_{Viscous} is found at the interfacial zone of two flows. The higher intensity of N'''_{Viscous} is found due to the existence of higher velocity gradient. At the interface of two flows, the directions of primary and secondary flows are opposite and generate higher intensity of N'''_{Viscous}.

To analyse the irreversibility associated with the heat transfer and fluid flow through the wavy channel, total entropy generation should be discussed. The variation of dimensionless total entropy generation $\left(N_{\text{Total}}\right)$ with Prandtl

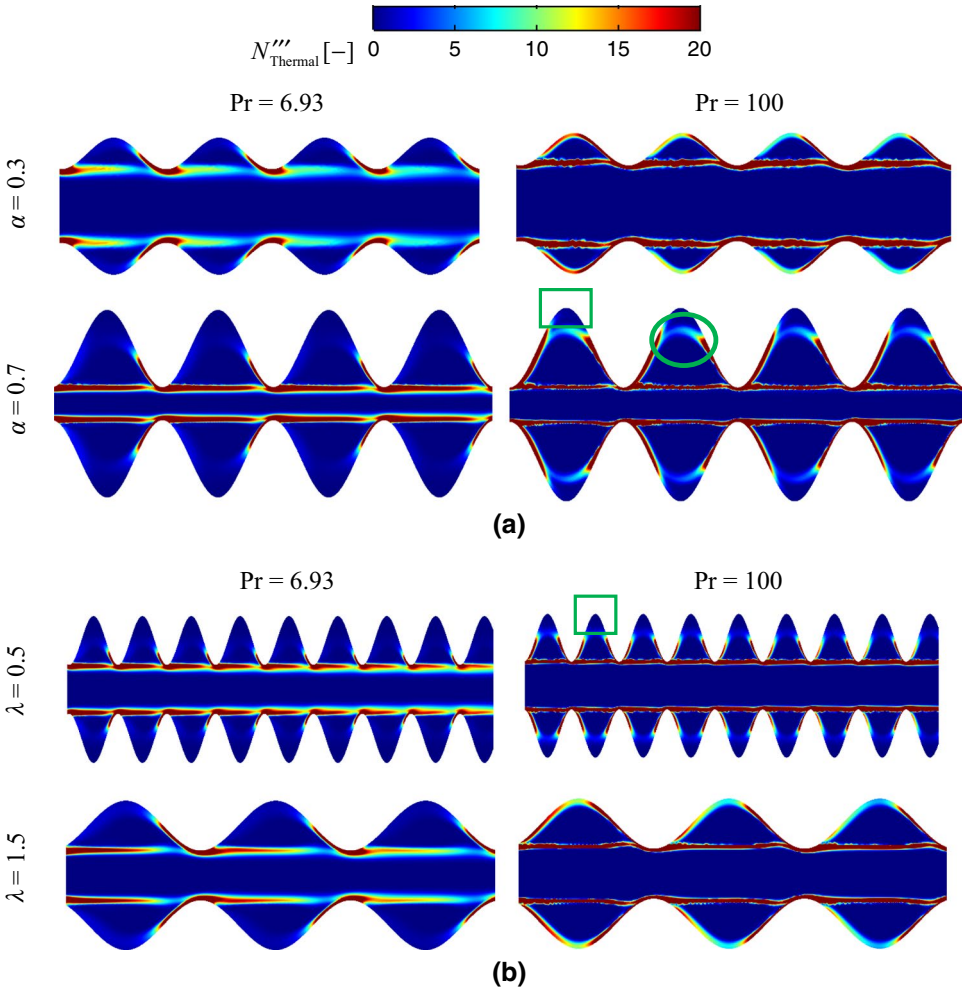

Fig. 11 **a** Dimensionless thermal entropy generation contour at different amplitudes with $\lambda = 1$ and Re = 100, **b** Dimensionless thermal entropy generation contour at different wavelengths with $\alpha = 0.5$ and Re = 100; for two values of Prandtl number: smaller Prandtl number (Pr = 6.93, left side) and higher Prandtl number (Pr = 100, right side)

number for Re = 25 (left) and 100 (right) is presented in Fig. 13 with different values of λ at $\alpha = 0.3$, 0.5 and 0.7 (top to bottom). It should be noted that in the present study, the order of viscous entropy generation is small (10^{-4} *to* 10^{-3}) compared to the contribution of average thermal entropy for the present study. Similar order of average viscous entropy generation is found from the literature for flow through wavy or corrugated channel in laminar regime [32, 46]. It can be seen from Fig. 13 that the N_{Total} increases with increase in Prandtl number for all values of α, λ and Re. It is because of the increase in local intensity of N'''_{Thermal} at throat region and increase in intensity of interfacial N'''_{Thermal} region with Prandtl number. The increase in Reynolds number also enhances N_{Total}, because of increase in temperature gradients at throat and flow interface through increase in advection strength. The increase in amplitude and decrease in wavelength enhance N_{Total} at higher values of Prandtl number, as increase in amplitude at higher Prandtl number enhances the temperature gradients. However, for Pr = 0.72, the increase in number of waves has not significant effect on N_{Total} as the higher intensity of N'''_{Thermal} only exists at the small region of throat for any Reynolds number. Similar effect can be observed with increase in amplitude for Pr = 0.72. It is because of the small increment of intensity of N'''_{Thermal} at throat with α at Pr = 0.72.

It can be noted that at smaller amplitude ($\alpha = 0.3$) and lower Reynolds number (Re = 25), the change in λ has insignificant effect on N_{Total} for all Prandtl number. For Re = 25, the variations of N_{Total} with λ are linear and exponential for $\alpha = 0.5$ and 0.7, respectively, for Pr $\geq$ 6.93, whereas for Re = 100, for $\alpha = 0.3$, the variation of N_{Total} with λ is linear, and for $\alpha = 0.5$ and 0.7, it is exponential for Pr $\geq$ 6.93. This exponential growth of N_{Total} at higher value of amplitude and Reynolds number can be explained by the fact that secondary and tertiary flow zones induce interfacial N'''_{Thermal} region and growth of N'''_{Thermal} region in diverging section.

For the present study, the total entropy generation is compared with the equivalent plane channel. To assess the irreversibility associated with heat transfer in wavy channel compared to plane channel, percentage difference in total entropy generation compared to plane channel $\left(\Delta N_{\text{Total},\%}\right)$ is analysed. Mathematically, it is defined as:

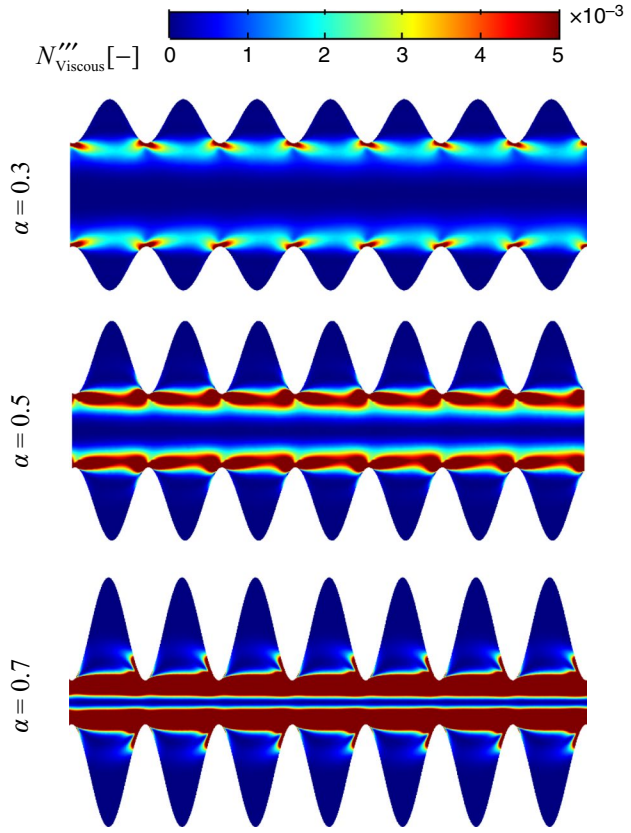

Fig. 12 Dimensionless viscous entropy generation contour at different amplitudes at Re = 100 and $\lambda = 0.5$

$\Delta N_{\text{Total},\%} = 100\left(N_{\text{Wavy}} - N_{\text{Plane}}\right)/N_{\text{Plane}}$. The variation of $\Delta N_{\text{Total},\%}$ with Prandtl number is presented in Fig. 14 for Re = 25 (left) and Re = 100 (right) and for different values of wavelength with $\alpha = 0.3$, 0.5 and 0.7 (top to bottom). It is found that for $\alpha = 0.3$ $\Delta N_{\text{Total},\%}$ varies non-monotonically with Prandtl number for lower Reynolds number (Re = 25) and any value of λ, whereas for higher Reynolds number (Re = 100), it has non-monotonic variation with Prandtl number only for higher λ. For $\alpha = 0.5$ and 0.7, $\Delta N_{\text{Total},\%}$ increases sharply up to Pr = 6.93 and increases gradually beyond it. For $\alpha = 0.3$ and Re = 25, $\Delta N_{\text{Total},\%}$ increases with Prandtl number up to Pr = 6.93 and decreases beyond that critical value. It can be explained as follows. For plane channel at Re = 25, the significant intensity of N'''_{Thermal} exists only near to the inlet side for Pr = 0.72 and 6.93, whereas for higher values of Prandtl number (Pr = 20, 50 and 100), the intensity of N'''_{Thermal} is significant at the wall from inlet to outlet section and its intensity increases with Prandtl number. On the other hand, for wavy channel with $\alpha = 0.3$, for lower Prandtl number (Pr = 0.72 and 6.93) the intensity of N'''_{Thermal} exists near the throat regions (see Fig. 10). With an increase in Prandtl number, N'''_{Thermal} intensity at throat increases and the secondary flow region allows nearly zero N'''_{Thermal} at trough. Some interfacial N'''_{Thermal} for two flow zone is also appeared for Pr = 50 and 100. However, at Re = 25, the recirculation strength is weaker; therefore, the intensity of interfacial N'''_{Thermal} is much lower than the throat. Hence, the combined effect is an increase in $\Delta N_{\text{Total},\%}$ up to Pr = 6.93 due to the higher value of N_{Total} for wavy channel as for smaller value of Prandtl number generates higher intensity of N'''_{Thermal} only near the inlet of plane channel and wavy channel for all throats. Note that $\Delta N_{\text{Total},\%}$ decreases beyond Pr = 6.93, as N_{Total} for plane channel increases as compared to wavy channel. Plane channel has higher intensity of N'''_{Thermal} throughout the channel length, whereas for wavy channel zero N'''_{Thermal} appears at trough section due to the recirculation zone. With decrease in λ, the interfacial intensity N'''_{Thermal} has significant contribution to enhance N_{Total} as number of undulation increases and this contribution is amplified when Prandtl number is increased. Therefore, for $\lambda = 1.5$, negative $\Delta N_{\text{Total},\%}$ is found for $50 \le \text{Pr} \le 100$; for $\lambda = 1$, negative $\Delta N_{\text{Total},\%}$ is found only at Pr = 100 and for $\lambda = 0.5$ $\Delta N_{\text{Total},\%}$ is positive for all values of Prandtl number. For Re = 100 and $\alpha = 0.3$, at $\lambda = 1.5$, the value of $\Delta N_{\text{Total},\%}$ decreases with Prandtl number up to Pr = 20 and increases beyond it, whereas for $\lambda = 1$ and 0.5, $\Delta N_{\text{Total},\%}$ monotonically increases with Prandtl number. This can be explained as follows. For higher Reynolds number (Re = 100), at $\lambda = 1.5$, the higher values of wavelength allow smaller interfacial N'''_{Thermal} as the smaller amplitude to wavelength ratio allows gradual wavy curvature and weaker temperature gradient for relatively gradual flow, whereas at smaller λ, higher amplitude to wavelength ratio allows sudden change in wavy curvature and abrupt change in flow allows higher intensity of N'''_{Thermal} near the interfacial flow regions. In addition, the increase in Prandtl number, local interfacial N'''_{Thermal} intensity is amplified. Therefore, at $\lambda = 1.5$ the combined effect decreases $\Delta N_{\text{Total},\%}$ up to Pr = 20 due to the small increment in difference of N_{Total} for plane and wavy channel with Prandtl number, whereas at smaller λ, the increase in interfacial N'''_{Thermal} intensity even at smaller Prandtl number in addition with generation of significant N'''_{Thermal} intensity at diverging section at higher Prandtl number allows to increase $\Delta N_{\text{Total},\%}$ monotonically with Prandtl number. For higher amplitude ($\alpha = 0.5$ and 0.7), the increase in intensity of N'''_{Thermal} at throat along with the effect of interfacial (primary and secondary flow, secondary and tertiary flow) intensity of N'''_{Thermal} and diverging section intensity of N'''_{Thermal} for higher Reynolds number allow higher total entropy generation over the plane channel. All these factors of enhancing the total entropy amplify at higher Prandtl number. Therefore, the maximum value of $\Delta N_{\text{Total},\%}$ is found 30–44% and 84–111% for $\alpha = 0.5$ and 0.7, respectively, when Reynolds number changes from 25 to 100. For $\alpha = 0.5$ and 0.7, $\Delta N_{\text{Total},\%}$ increases sharply with Prandtl number up to

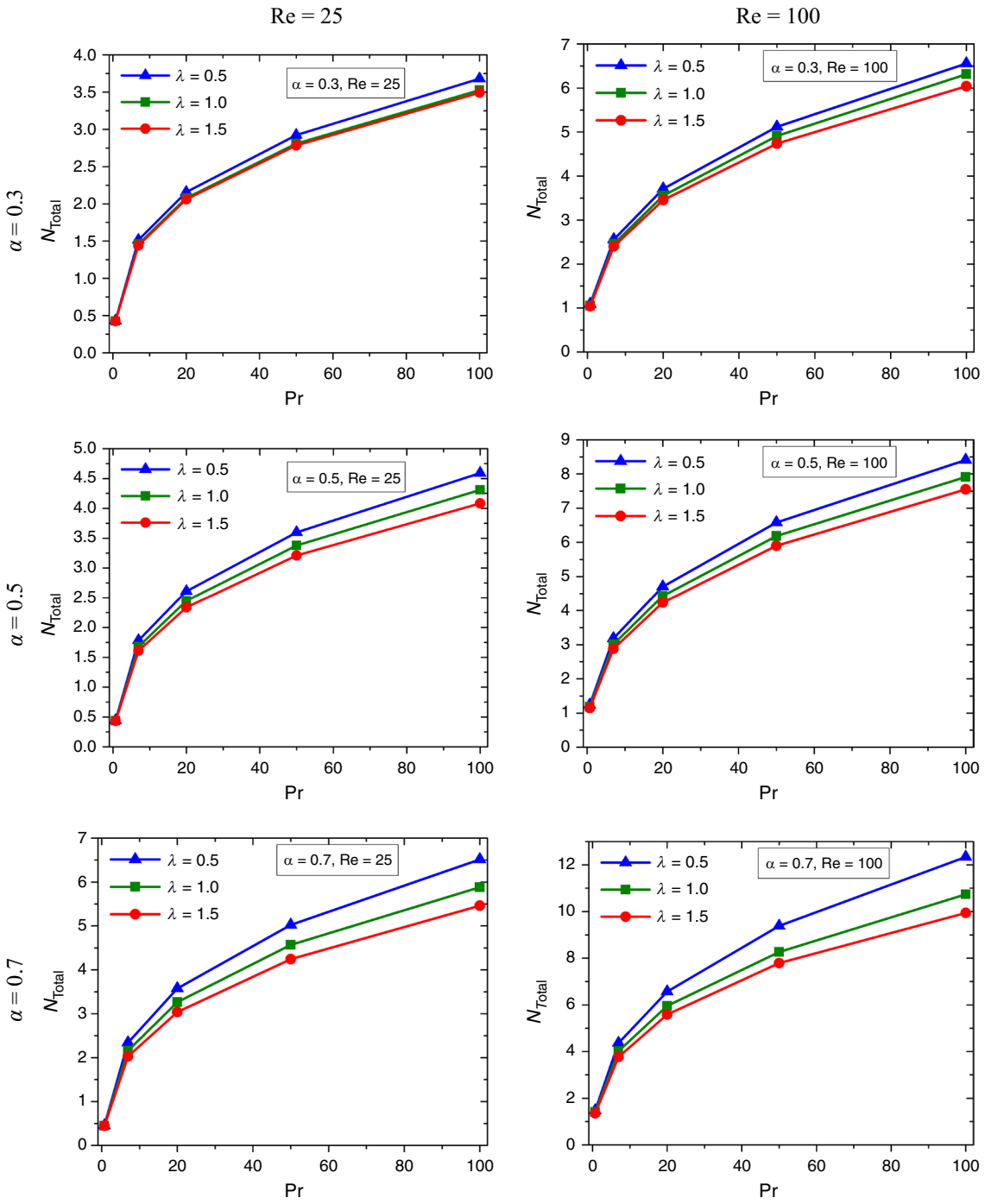

Fig. 13 Dimensionless total entropy generation versus Prandtl number for different values of wavelength for Re = 25 (left) and 100 (right) for $\alpha = 0.3$, 0.5 and 0.7 (top to bottom)

Pr = 6.93, as for Pr = 0.72, negligible or smaller intensity of N'''_{Thermal} is found at any interfacial zone, whereas significant value of interfacial N'''_{Thermal} for Pr = 6.93 allows sudden increment in N_{Total}. Therefore, $\Delta N_{\text{Total},\%}$ increases sharply up to Pr = 6.93. Beyond this limit, the increase in $\Delta N_{\text{Total},\%}$ with Prandtl number is gradual as the core zero thermal entropy generation region is also expanded towards the wall with Prandtl number with other factor which increases the value of N_{Total} of wavy channel.

As the smaller irreversibility compared to plane channel is found for $\alpha = 0.3$, therefore the variation of $\Delta N_{\text{Total},\%}$ with Reynolds number for all Prandtl number is presented in Fig. 15 at $\lambda = 0.5$ to 1.5. It can be seen that for all λ, the increase in $\Delta N_{\text{Total},\%}$ is found with Reynolds number

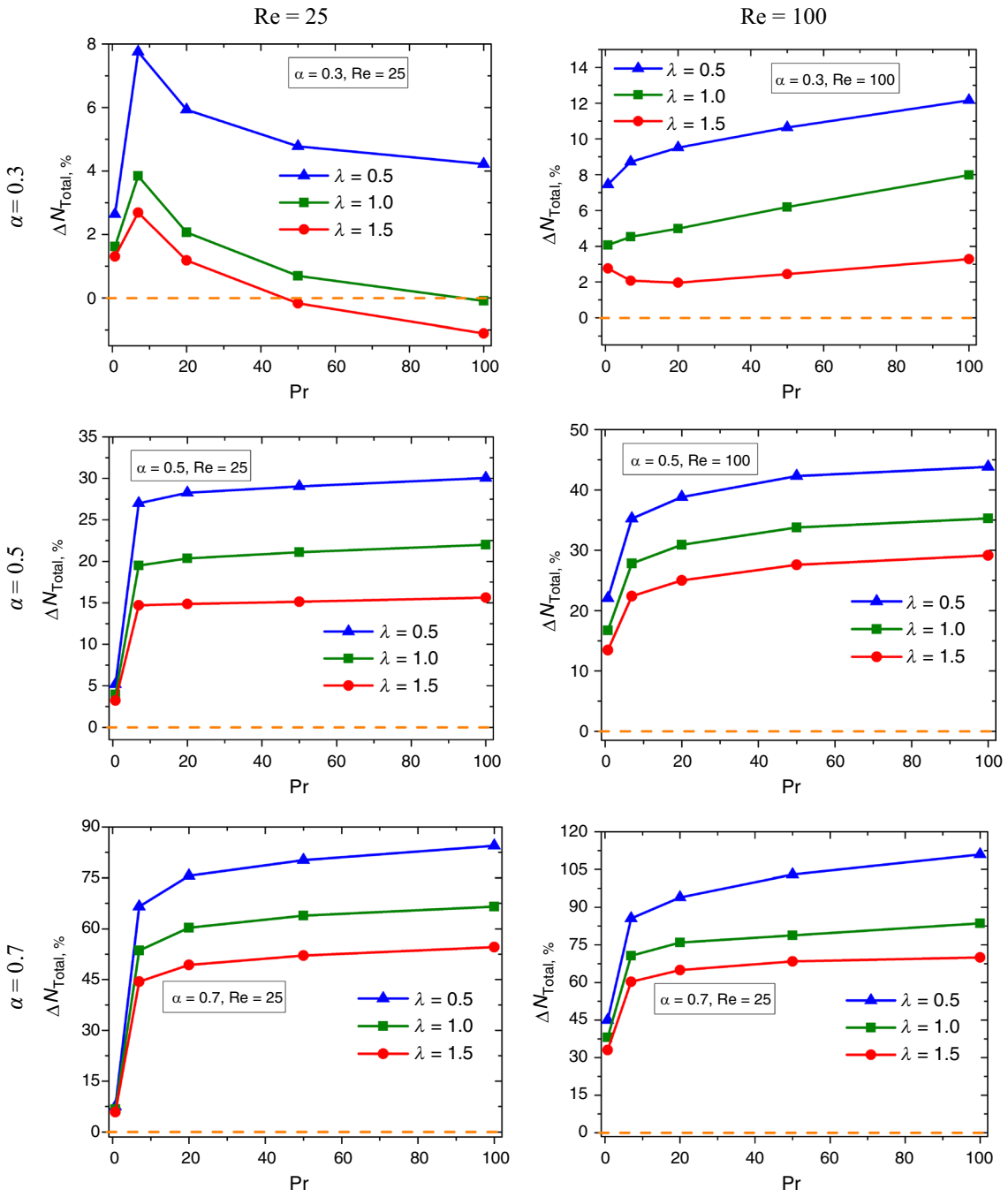

Fig. 14 Percentage difference in total entropy generation of wavy channel relative to equivalent plane channel versus Prandtl number for different values of wavelength for Re = 25 (left) and 100 (right) for $\alpha = 0.3$, 0.5 and 0.7 (top to bottom)

monotonically for Pr = 0.72, whereas for higher Prandtl number $\Delta N_{\text{Total},\%}$ decreases up to the critical Reynolds number and again increases for all λ except for the case of Pr = 6.93. The variation can be explained as follows. For all cases at Re = 5, the increase in Prandtl number increases $\Delta N_{\text{Total},\%}$ up to Pr = 20 and decreases beyond it. It is because at Re = 5, the sharp increase in difference in N_{Total} for plane and wavy channel is found for $0.72 \leq \text{Pr} \leq 20$, whereas N_{Total} increases exponentially for all Prandtl number for plane channel. Hence, the overall effect increases it up to Pr = 20 and decreases beyond it. It can be noted that for Pr = 0.72 at Re = 5, the value of $\Delta N_{\text{Total},\%}$ is zero for all values of λ. It is because of the existence of N'''_{Thermal} intensity for both wavy and plane channel only at small part near the inlet wall. Therefore, the difference in N_{Total} for plane and wavy channel is so small and leads to zero $\Delta N_{\text{Total},\%}$. The difference

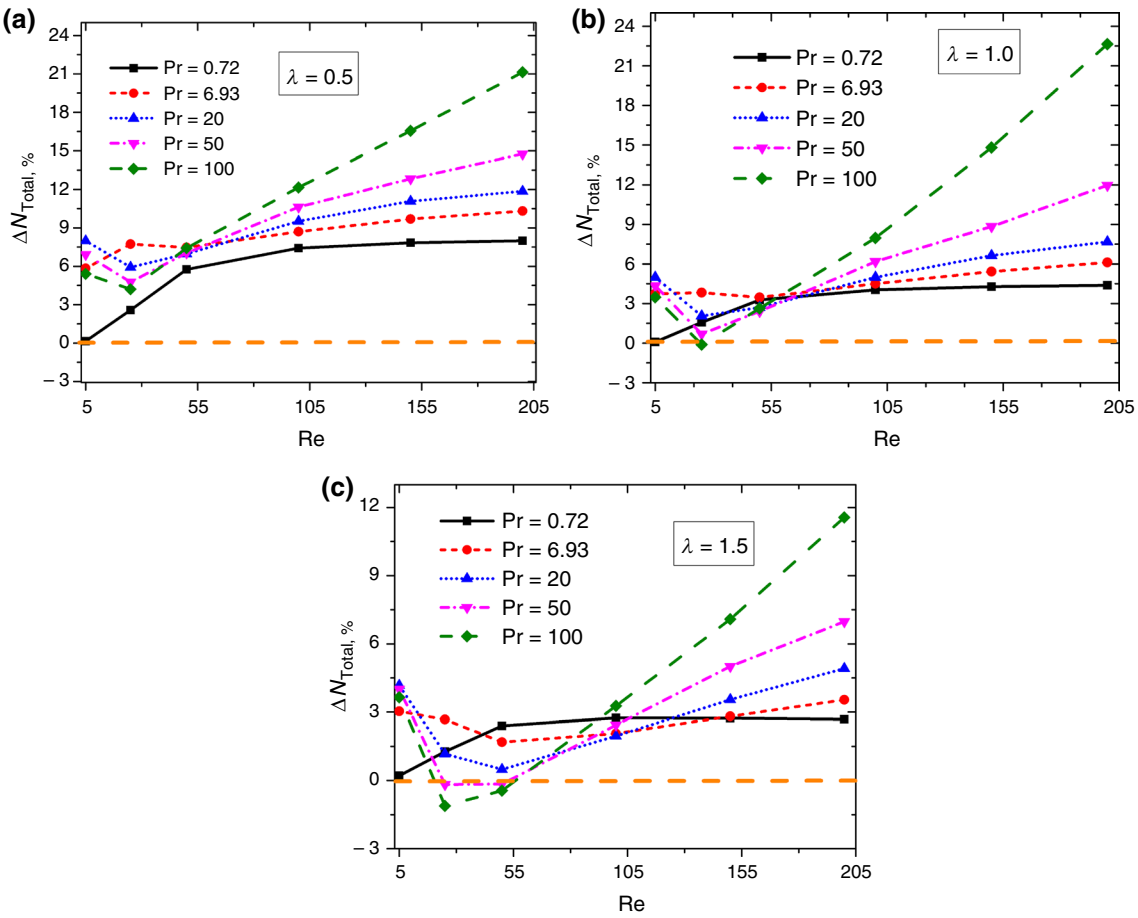

Fig. 15 Percentage difference in total entropy generation of wavy channel relative to equivalent plane channel versus Reynolds number for different values of Prandtl number with $\alpha = 0.3$

in N_{Total} for plane and wavy channel for Pr = 0.72 is nearly zero for Re = 25 as for this case the significant intensity of N'''_{Thermal} is found only for two wavelengths for wavy channel and small region near the wall of plane channel. For $\lambda = 0.5$, with increase in Reynolds number up to Re = 25, the difference in N_{Total} for plane and wavy channel increases sharply for Pr = 6.93 and gradually for Pr = 20 to 100, whereas the increase in N_{Total} for plane channel is very high for all Prandtl number. For Pr = 6.93, all wavy throats have significant intensity of N'''_{Thermal} and for higher Prandtl number (Pr > 6.93) only flow interfacial N'''_{Thermal} intensity increases with Prandtl number significantly. Hence, the combined effect increases $\Delta N_{\text{Total},\%}$ sharply with Reynolds number for Pr = 6.93 and decreases for Pr > 6.93 up to Re = 25. For Re > 25, the magnitude of difference in N_{Total} for all values of Prandtl number increases sharply compared to increase in N_{Total} of plane channel. At higher Reynolds number, there are multiple locations of growth of N'''_{Thermal} as already discussed. For $\lambda = 1$ the difference in N_{Total} for plane and wavy channel increases for Pr < 6.93 and decreases for higher values of Prandtl number (Pr > 6.93), with Reynolds number up to Re = 25. The rate of decrement in difference of N_{Total} with Reynolds number up to Re = 25 increases with Prandtl number. It is because of the recirculation zone, which creates zero N'''_{Thermal} region in wavy channel along with the small number of recirculation zone at $\lambda = 1$ compared to $\lambda = 0.5$. On the other hand, for plane channel, the thickness of significant intensity of N'''_{Thermal} increases with Prandtl number. Combined effect allows the decrement in difference of N_{Total} and attains some negative value for Pr = 100 at Re = 25. The discussed effect is visible in corresponding plot of $\Delta N_{\text{Total},\%}$ at $\lambda = 1$. Beyond Re > 25, the difference in N_{Total} for plane and wavy channel increases with Reynolds number. Hence, the same effect is also visible on $\Delta N_{\text{Total},\%}$ for Re > 25.

For the case of $\lambda = 1.5$, less number of waves allows smaller accumulation of interfacial N'''_{Thermal} intensity. Hence, the difference in N_{Total} for plane and wavy channel is negative for two higher values of Prandtl number (Pr = 50 and 100). For Pr = 100, the difference is negative in the range of $25 \leq \text{Re} \leq 50$ and for Pr = 50 at Re = 25. The corresponding effects are visible in the plot of $\Delta N_{\text{Total},\%}$ at $\lambda = 1.5$. For this case, the variation of $\Delta N_{\text{Total},\%}$ is similar for the case of $\lambda = 1$.

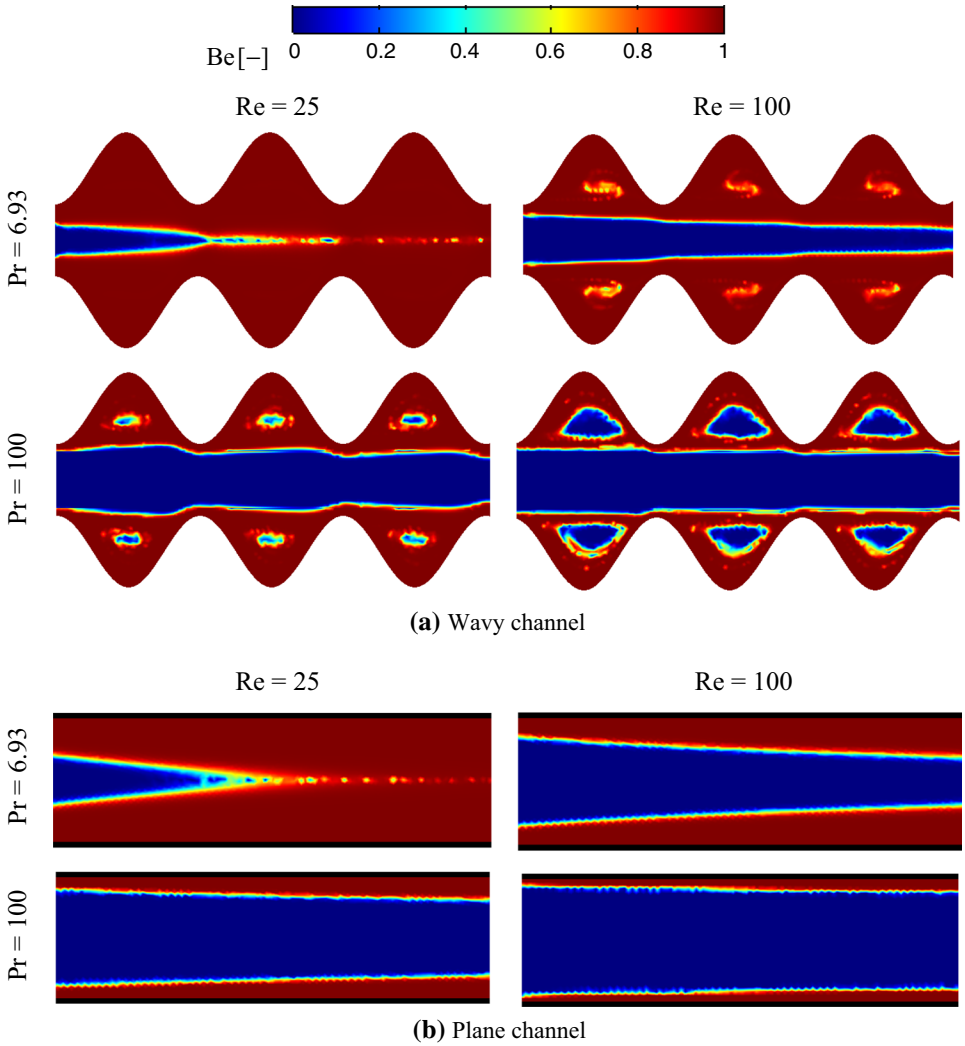

Fig. 16 Bejan number contour for higher (Pr = 6.93, top) and lower (Pr = 100, bottom) value of Prandtl number for (a) wavy channel with $\alpha = 0.5$ and $\lambda = 1$, and (b) Plane channel, with higher (Re = 25, left side) and lower Reynolds number (Re = 100, right side)

Figure 16 depicts the local variation of Bejan number for wavy and plane channel at Pr = 6.93 and 100 with two values of Reynolds number equal to 25 and 100. The zero Bejan number cone is appeared in the core for all geometry as the core cold fluid creates zero thermal entropy region. This cone has grown to rectangular shape when Prandtl number increases to 6.93–100 for any geometry and Reynolds number. It is because of the fact that increase in Prandtl number allows higher thermal entropy generation region only near to the wall for given geometry and Reynolds number. It can be noted that the zero Bejan number cone is smaller for wavy channel for any Reynolds number and Prandtl number. It is because of the existence of wavy throat, the significant magnitude of Bejan number is found in the core region for the case of wavy channel. It is important to mention that at Re = 25 and Pr = 6.93, there is no decrement in Bejan number inside the trough section, whereas for Re = 25 and Pr = 6.93, small intensity of Bejan number is found in trough section. It is because at Re = 25 and Pr = 6.93, the intensity of thermal entropy generation is so small in trough due to the recirculation zone compared to the throat thermal entropy generation intensity (as we named this region as "zero thermal entropy generation region" on the basis of relative magnitude of thermal entropy generation at throat); however, the order of viscous entropy generation is much less than the smaller intensity of thermal entropy generation in this region. Therefore, unity Bejan number in trough is found for this case. For the case of Pr = 6.93 and Re = 100, the relative decrement in thermal entropy generation in recirculation zone as temperature uniformity enhances in this region. Therefore, moderate value of Bejan number is found for this region. For the case of Pr = 100, for both Re = 25 and 100, the exactly zero thermal entropy generation in recirculation zone allows zero intensity of Bejan number. This zero Bejan number region at trough is expanded with Reynolds number as it enhances temperature uniformity and expands the zero thermal entropy generation region.

Conclusions

The thermo-hydraulic and entropy generation analyses are carried out for flow of Newtonian fluid through the wavy channel by varying the amplitude, wavelength, Reynolds number and Prandtl number. The effects of these parameters on the flow and temperature fields are discussed in terms of contours of streamlines and isotherms, Nusselt number, enhancement ratio, pressure drop, performance factor, thermal entropy generation, viscous entropy generation and total entropy generation. The main findings from the present work are summarized as follow:

- The decrement of the thickness of the thermal boundary layer with Prandtl number at trough is less compared to throat for lower Reynolds number. The average Nusselt number increases with Prandtl number for all the geometrical configurations.
- For smaller Reynolds number, enhancement ratio (ER) increases with Prandtl number, attains a maximum value at critical Prandtl number (Pr_c) and decreases again with further increase in Pr. Critical Prandtl number is independent of wavelength and depends on the amplitude. The value of Pr_c is higher for higher amplitude. For higher Reynolds number, ER monotonically increases with Prandtl number.
- At lower Re, the performance factor (PF) shows a non-monotonic trend with Prandtl number, whereas at higher Reynolds number, it monotonically increases with Prandtl number for any given combination of the geometrical parameters. For a given amplitude, the decrease in λ causes non-monotonic variation of PF with Reynolds number at higher values of Prandtl number and moreover, PF decreases up to the critical Re (Re_c) and increases again. The value of Re_c shows a decreasing trend with increase in amplitude.
- Local thermal entropy generation ($N'''_{Thermal}$) is always higher at the throat of the wavy channel and increases its value with increase in Reynolds number or Prandtl number. The higher intensity of $N'''_{Thermal}$ region is expanded along the wavy wall converging section towards upstream with increase in Prandtl number. At higher Reynolds number and Prandtl number, the significant intensity of $N'''_{Thermal}$ is also found in the diverging section and its intensity increases with Prandtl number. For higher Reynolds number, the interface between secondary and tertiary flow creates significant intensity of $N'''_{Thermal}$ and its intensity increases with Prandtl number.
- Total entropy generation (N_{Total}) increases with increase in amplitude and wavelength, Reynolds number and Prandtl number. For higher amplitude and Reynolds number, N_{Total} increases exponentially, whereas it is linear for smaller amplitude and Reynolds number.
- For $\alpha = 0.3$, the irreversibility is smaller as compared to the plane channel. The difference in total entropy generation ($\Delta N_{Total,\%}$) for plane and wavy channel is negative for two higher values of Prandtl number (Pr = 50 and 100) at higher wavelength with $\alpha = 0.3$.
- The zero Bejan number cone is present at the core region of the channel. This core region expands with Reynolds number and Prandtl number. This zone is smaller for wavy channel compared to the plane channel. For higher value of Reynolds number and Prandtl number, zero Bejan number zone is induced inside the recirculation zone.

Acknowledgements The authors acknowledge TEQIP-III, NIT Silchar for its support throughout the work.

References

1. Shamsabadi H, Rashidi S, Esfahani JA. Entropy generation analysis for nanofluid flow inside a duct equipped with porous baffles. J Therm Anal Calorim. 2019;135:1009–19.
2. Menni Y, Azzi A, Chamkha A. Enhancement of convective heat transfer in smooth air channels with wall-mounted obstacles in the flow path: a review. J Therm Anal Calorim. 2019;135:1951–76.
3. Hosseinirad E, Hormozi F. Thermal performance enhancement in a miniature channel using different passive methods. J Therm Anal Calorim. 2019;135:1849–61.
4. Gawande VB, Dhoble AS, Zodpe DB. Effect of roughness geometries on heat transfer enhancement in solar thermal systems—a review. Renew Sustain Energy Rev. 2014;32:347–78.
5. Kareem ZS, Mohd Jaafar MN, Lazim TM, Abdullah S, Abdulwahid AF. Passive heat transfer enhancement review in corrugation. Exp Therm Fluid Sci. 2015;68:22–38.
6. Kurtulmuş N, Sahin B. A review of hydrodynamics and heat transfer through corrugated channels. Int Commun Heat Mass Transf. 2019;108:104307.
7. Mousavi SM, Biglarian M, Darzi AAR, Farhadi M, Afrouzi HH, Toghraie D. Heat transfer enhancement of ferrofluid flow within a wavy channel by applying a non-uniform magnetic field. J Therm Anal Calorim. 2019. https://doi.org/10.1007/s10973-019-08650-6.
8. Khoshvaght-Aliabadi M, Ariana H, Khaligh SF, Salami M. Effects of delta winglets on performance of wavy plate-fin in PFHEs: nanofluid as heat transfer media. J Therm Anal Calorim. 2018;131:1625–40.
9. Bhowmick D, Randive PR, Pati S. Effect of thickness of porous layer on thermo-hydraulic characteristics and entropy generation in a partially porous wavy channel. In: Biswal B, Sarkar B, Mahanta P, editors. Advances in mechanical engineering., Lecture notes in mechanical engineeringSingapore: Springer; 2020. https://doi.org/10.1007/978-981-15-0124-1_13.
10. Rashidi S, Akbarzadeh M, Karimi N, Masoodi R. Combined effects of nanofluid and transverse twisted-baffles on the flow structures, heat transfer and irreversibilities inside a square duct—a numerical study. Appl Therm Eng. 2018;130:135–48.

11. Boruah MP, Pati S, Randive PR. Implication of fluid rheology on the hydrothermal and entropy generation characteristics for mixed convective flow in a backward facing step channel with baffle. Int J Heat Mass Transf. 2019;137:138–60.
12. Boruah MP, Randive PR, Pati S. Hydrothermal performance and entropy generation analysis for mixed convective flows over a backward facing step channel with baffle. Int J Heat Mass Transf. 2019;125:525–42.
13. Javadi H, Mousavi Ajarostaghi SS, Pourfallah M, Zaboli M. Performance analysis of helical ground heat exchangers with different configurations. Appl Therm Eng. 2019;154:24–36.
14. Toghraie D, Abdollah MMD, Pourfattah F, Akbari OA, Ruhani B. Numerical investigation of flow and heat transfer characteristics in smooth, sinusoidal and zigzag-shaped microchannel with and without nanofluid. J Therm Anal Calorim. 2018;131:1757–66.
15. Feizabadi A, Khoshvaght-Aliabadi M, Rahimi AB. Experimental evaluation of thermal performance and entropy generation inside a twisted U-tube equipped with twisted-tape inserts. Int J Therm Sci. 2019;145:106051.
16. Akbarzadeh M, Rashidi S, Bovand M, Ellahi R. A sensitivity analysis on thermal and pumping power for the flow of nanofluid inside a wavy channel. J Mol Liq. 2016;220:1–13.
17. Esfahani JA, Akbarzadeh M, Rashidi S, Rosen MA, Ellahi R. Influences of wavy wall and nanoparticles on entropy generation over heat exchanger plat. Int J Heat Mass Transf. 2017;109:1162–71.
18. Sajid MU, Ali HM, Sufyan A, Rashid D, Zahid SU, Rehman WU. Experimental investigation of TiO_2–water nanofluid flow and heat transfer inside wavy mini-channel heat sinks. J Therm Anal Calorim. 2019;137:1279–94.
19. Akbarzadeh M, Rashidi S, Karimi N, Omar N. First and second laws of thermodynamics analysis of nanofluid flow inside a heat exchanger duct with wavy walls and a porous insert. J Therm Anal Calorim. 2019;135:177–94.
20. Singh S. Experimental and numerical investigations of a single and double pass porous serpentine wavy wiremesh packed bed solar air heater. Renew Energy. 2020;145:1361–87.
21. Lin W, Ren H, Ma Z. Mathematical modelling and experimental investigation of solar air collectors with corrugated absorbers. Renew Energy. 2020;145:164–79.
22. Rashidi S, Javadi P, Esfahani JA. Second law of thermodynamics analysis for nanofluid turbulent flow inside a solar heater with the ribbed absorber plate. J Therm Anal Calorim. 2019;135:551–63.
23. Akbarzadeh M, Rashidi S, Karimi N, Ellahi R. Convection of heat and thermodynamic irreversibilities in two-phase, turbulent nanofluid flows in solar heaters by corrugated absorber plates. Adv Powder Technol. 2018;29:2243–54.
24. Mohanraj M, Jayaraj S, Muraleedharan C. Applications of artificial neural networks for thermal analysis of heat exchangers—a review. Int J Therm Sci. 2015;90:150–72.
25. Mohanraj M, Gunasekar N, Velmurugan V. Comparison of energy performance of heat pumps using a photovoltaic-thermal evaporator with circular and triangular tube configurations. Build Simul. 2016;9:27–41.
26. Kumar RA, Babu BG, Mohanraj M. Thermodynamic performance of forced convection solar air heaters using pin–fin absorber plate packed with latent heat storage materials. J Therm Anal Calorim. 2016;126:1657–78.
27. Yerdesh Y, Abdulina Z, Aliuly A, Belyayev Y, Mohanraj M, Kaltayev A. Numerical simulation on solar collector and cascade heat pump combi water heating systems in Kazakhstan climates. Renew Energy. 2020;145:1222–34.
28. Arun KR, Kunal G, Srinivas M, Kumar CSS, Mohanraj M, Jayaraj S. Drying of untreated Musa nendra and Momordica charantia in a forced convection solar cabinet dryer with thermal storage. Energy. 2020;192:116697.
29. Rush TA, Newell TA, Jacobi AM. An experimental study of flow and heat transfer in sinusoidal wavy passages. Int J Heat Mass Transf. 1999;42:1541–53.
30. Wang CC, Chen CK. Forced convection in a wavy-wall channel. Int J Heat Mass Transf. 2002;45:2587–95.
31. Pati S, Mehta SK, Borah A. Numerical investigation of thermo-hydraulic transport characteristics in wavy channels: comparison between raccoon and serpentine channels. Int Commun Heat Mass Transf. 2017;88:171–6.
32. Mehta SK, Pati S. Analysis of thermo-hydraulic performance and entropy generation characteristics for laminar flow through triangular corrugated channel. J Therm Anal Calorim. 2019;136:49–62.
33. Singh V, Haridas D, Srivastava A. Experimental study of heat transfer performance of compact wavy channel with nanofluids as the coolant medium: real time non-intrusive measurements. Int J Therm Sci. 2019;145:105993.
34. Kareem A, Rahim A, Talib A, Acosta A, Thariq M, Sultan H, et al. Effect of corrugated wall combined with backward-facing step channel on fluid flow and heat transfer. Energy. 2020;190:116294.
35. Ould-Rouiss M, Redjem-Saad L, Lauriat G, Mazouz A. Effect of Prandtl number on the turbulent thermal field in annular pipe flow. Int Commun Heat Mass Transf. 2010;37:958–63.
36. Nath D, Raju BHS, Pati S. Effect of Prandtl number on thermo-fluidic transport characteristics for mixed convection past a sphere. Int Commun Heat Mass Transf. 2018;98:191–9.
37. Rahman MM, Parvin S, Rahim NA, Islam MR, Saidur R, Hasanuzzaman M. Effects of Reynolds and Prandtl number on mixed convection in a ventilated cavity with a heat-generating solid circular block. Appl Math Model. 2012;36:2056–66.
38. Chatterjee D, Sinha C. Effect of Prandtl number and rotation on vortex shedding behind a circular cylinder subjected to cross buoyancy at subcritical Reynolds number. Int Commun Heat Mass Transf. 2016;70:1–8.
39. Mirzaei M, Davidson L, Sohankar A, Innings F. The effect of corrugation on heat transfer and pressure drop in channel flow with different Prandtl numbers. Int J Heat Mass Transf. 2013;66:164–76.
40. Kumar A, Dhiman A, Baranyi L. Fluid flow and heat transfer around a confined semi-circular cylinder: onset of vortex shedding and effects of Reynolds and Prandtl numbers. Int J Heat Mass Transf. 2016;102:417–25.
41. Shyam R, Chhabra RP. Effect of Prandtl number on heat transfer from tandem square cylinders immersed in power-law fluids in the low Reynolds number regime. Int J Heat Mass Transf. 2013;57:742–55.
42. García A, Vicente PG, Viedma A. Experimental study of heat transfer enhancement with wire coil inserts in laminar-transition-turbulent regimes at different Prandtl numbers. Int J Heat Mass Transf. 2005;48:4640–51.
43. Selimefendigil F, Oztop HF, Mahian O. Effects of a partially conductive partition in MHD conjugate convection and entropy generation for a horizontal annulus. J Therm Anal Calorim. 2020;139:1537–51.
44. Bondarenko DS, Sheremet MA, Oztop HF, Ali ME. Impacts of moving wall and heat-generating element on heat transfer and entropy generation of Al_2O_3/H_2O nanofluid. J Therm Anal Calorim. 2019;136:673–86.
45. Sekrani G, Poncet S, Proulx P. Conjugated heat transfer and entropy generation of Al_2O_3–water nanofluid flows over a heated wall-mounted obstacle. J Therm Anal Calorim. 2019;135:963–79.
46. Akbarzadeh M, Rashidi S, Esfahani JA. Influences of corrugation profiles on entropy generation, heat transfer, pressure drop, and performance in a wavy channel. Appl Therm Eng. 2017;116:278–91.

47. Pati S, Som SK, Chakraborty S. Thermodynamic performance of microscale swirling flows with interfacial slip. Int J Heat Mass Transf. 2013;57:397–401.
48. Pati S, Roy R, Deka N, Boruah MP, Nath M, Bhargav R, Randive PR, Mukherjee PP. Optimal heating strategy for minimization of peak temperature and entropy generation for forced convective flow through a circular pipe. Int J Heat Mass Transf. 2020;150:119318.
49. Magherbi M, Abbassi H, Brahim AB. Entropy generation at the onset of natural convection. Int J Heat Mass Transf. 2003;46:3441–50.
50. Khan I, Khan WA, Qasim M, Afridi I, Alharbi SO. Thermodynamic analysis of entropy generation minimization in thermally dissipating flow over a thin needle moving in a parallel free stream of two Newtonian fluids. Entropy. 2019;21:74. https://doi.org/10.3390/e21010074.
51. Bejan A. A study of entropy generation in fundamental convective heat transfer. J Heat Transf. 1979;101:718–25.
52. Fluent I, ANSYS FLUENT 14: theory guide Fluent Inc, Canonsburg, PA, USA; 2012.
53. Patankar SV. Numerical heat transfer and fluid flow. New York: McGraw-Hill; 1980.
54. Kumar A, Dhiman AK. Effect of a circular cylinder on separated forced convection at a backward-facing step. Int J Therm Sci. 2012;52:176–85. https://doi.org/10.1016/j.ijthermalsci.2011.09.014.
55. Farhanieh B, Herman Č, Sundén B. Numerical and experimental analysis of laminar fluid flow and forced convection heat transfer in a grooved duct. Int J Heat Mass Transf. 1993;36:1609–17.
56. Esfahani JA, Shahabi PB. Effect of non-uniform heating on entropy generation for the laminar developing pipe flow of a high Prandtl number fluid. Energy Convers Manag. 2010;51:2087–97.
57. Mondal B, Mehta SK, Patowari PK, Pati S. Numerical study of mixing in wavy micromixers: comparison between raccoon and serpentine mixer. Chem Eng Process Process Intensif. 2019;136:44–61.
58. Mehta SK, Pati S. Effect on non-uniform heating on heat transfer characteristics in wavy channel. In: Fifth international conference on computational methods for thermal problems ThermaComp 2018, Indian Institute of Science, Bangalore, Fifth Edition, July 2018, pp. 498–501.
59. Saikia A, Dalal A, Pati S. Thermo-hydraulic transport characteristics of non-Newtonian fluid flows through corrugated channels. Int J Therm Sci. 2018;129:201–8.
60. Pahlevaninejad N, Rahimi M, Gorzin M. Thermal and hydrodynamic analysis of non-Newtonian nanofluid in wavy microchannel. J Therm Anal Calorim. 2020. https://doi.org/10.1007/s10973-019-09229-x.
61. Bejan A. Convective heat transfer. 4th ed. Hoboken, NJ: Wiley; 2013.